# Dynamics of Snow and Glacier Cover in the Upper Karnali Basin, Nepal: An Analysis of Its Relationship with Climatic and Topographic Parameters

**Motilal Ghimire**[1]*, Dibas Shrestha[2], Raju Chauhan[3], Amrit Thapa[4], Til Prasad Pangali Sharma[5], Krishna Prasad Sharma[6], Sher Bahadur Gurung[6], Sundar Devkota[7], Prabin Bhandari[8], Sikesh Koirala[7], Yanhong Wu[9], Niroj Timalsina[6], and Jeevan Kutu[6]

[1] *Corresponding Author:* Tribhuvan University, Central Department of Geography, Kathmandu, Nepal. Email: motighimire@gmail.com

[2] Tribhuvan University, Central Department of Hydrology and Meteorology, Kathmandu, Nepal

[3] Tribhuvan University, Central Department of Environmental Science, Kathmandu, Nepal

[4] University of Alaska Fairbanks, Fairbanks, USA

[5] Tribhuvan University, Nepal Mountain Academy, Kathmandu, Nepal

[6] Tribhuvan University, Central Department of Geography, Kathmandu, Nepal

[7] Department of Survey, Government of Nepal, Kathmandu, Nepal

[8] George Mason University, Fairfax, Virginia, USA

[9] Institute of Mountain Hazards and Environment, Chinese Academy of Sciences, Chengdu, China

## Abstract

Snow and glacier cover in the Upper Karnali Basin (UKB) are crucial freshwater reservoirs that support downstream ecosystems and human populations. This study uses remote sensing and GIS data from various sources, MODIS-derived land surface temperature, and ERA5 reanalysis climate datasets to analyze snow cover dynamics from 2002 to 2024. The results show a

significant decrease in snow-covered area (SCA), with an annual decline of about 3.99 km². Seasonal variations indicate the most significant reductions during the monsoon period (July–September), where rising temperatures accelerate snowmelt. The analysis also establishes a strong negative correlation between snow cover and temperature ($r = -0.59$ to $-0.77$, $p < 0.05$), with warming trends disproportionately affecting mid-to-high elevation zones (3000-5000 m a.s.l.). Glacier basins exhibit consistent retreat, with the mean glacier area declining from 119.05 hectares in 2000 to 100.47 hectares in 2023, highlighting the impact of climate change. Additionally, snowline analysis demonstrates an upward migration, with the 10th percentile snowline increasing at a rate of approximately 5.16 m/year, which indicates progressive snow loss at lower elevations. Given the current warming trends (~0.0643°C/year above 5000 m a.s.l.), the UKB could experience a decline of glacier area by 47–69 % and snow-covered area by 19–30 %. These findings emphasize the vulnerability of UKB's cryosphere to climate change, necessitating adaptive water resource management strategies. This will help mitigate impacts on hydrology, agriculture, and regional water security.

**Keywords:** Snow and Glacier, Karnali, Himalayas, Remote Sensing, Climate Change, Elevation-depended-warming, Snowline

## 1. Introduction

Snow and glaciers in the mountains act as freshwater towers. Their meltwater provides a consistent supply to rivers and downstream ecosystems (Immerzeel et al., 2020; Wester et al., 2019; Pritchard, 2019). The meltwater from Himalayan ice and snow supports the livelihoods of millions across Nepal, India, and China by supplying drinking water, irrigation, hydropower, and ecosystem services (Bolch, 2007; Bookhagen and Burbank, 2010). Therefore, a decline in snow and glacier extent threatens water availability, food security, and sustainable development in these regions (Krishnan et al., 2019).

Furthermore, snow and glacial ice regulate regional and global climates by reflecting solar radiation, thereby contributing to the Earth's energy balance and influencing local weather patterns (Xu et al., 2009). Seasonal meltwater sustains ecosystems that provide habitats for numerous animal and plant species in mountainous regions. Consequently, changes in snow cover and glaciers can disrupt these entirely (Wester et al., 2019). On both local and regional scales, variations in the amount of snow and ice can contribute to changes in sea level, affecting coastal areas (Forster et al., 2021; Mimura, 2013; NOAA, 2013)

Snow-covered peaks and glaciers are major hubs for adventure, religious, and nature-based tourism (Anup, 2017; Nyaupane and Chhetri, 2009). Being sensitive to climate change, changes in their size and volume not only serve as visible indicators of broader climate trends but also directly threaten the tourism economy they support (Elsasser and Bürki, 2002).

A comprehensive understanding of cryospheric transformations is essential for accurate hydrological forecasting, assessing cryospheric hazards, and developing effective adaptation strategies. Historically, monitoring snow and glacier dynamics in the remote Himalayan regions

was limited by a scarcity of in-situ observations. Since the 1970s, advances in satellite remote sensing have revolutionized large-scale cryospheric assessments (Kääb et al., 2012; Muhammad and Thapa, 2020). The synergistic integration of satellite-derived data with sophisticated climate models and targeted ground-based measurements has subsequently enabled improved understanding of snow and glacier mass balance changes, their resultant hydrological impacts, and spatiotemporal variability (Bajracharya et al., 2014; Bolch et al., 2012; Gurung et al., 2017; Kääb et al., 2012; Krishnan et al., 2019; Kulkarni et al., 2021). Collectively, these studies demonstrate substantial snow and glacier loss across the Himalayas, altering river discharge seasonality and water resource availability

Extensive research on glaciers, glacier lakes, and glacier lake outburst floods (GLOFs) in Nepal has been conducted (Bajracharya et al., 2008; Hall et al., 2002; Kääb et al., 2005; Shrestha et al., 2012; Zemp, 2006). However, these studies disproportionately focus on the central and eastern Himalayas. The mid-western and far-western regions remain underrepresented due to their remoteness and limited accessibility (Shrestha et al., 2019; Khadka et al., 2024). Although global and regional glacier inventories specifically addressing high-resolution ($\leq$ 30 m) glacier cover remain limited (Bajracharya et al., 2014; Bolch et al., Analyses of elevation-dependent warming (EDW) and trend analyses are also scarce in the Himalayas (Pepin et al., 2015; Pepin et al., 2022; Desinayak et al., 2022). Furthermore, integrated studies linking glaciers, glacier basins, and snow cover to climate remain underexplored.

Bridging this gap is crucial for understanding cryosphere dynamics and their impacts on hydrology, hazards, and livelihoods in western Nepal. The Karnali Basin, Nepal's largest river basin (~40,780 km² upstream of the Chisapani gauge station) and home to approximately 2.5 million people (CBS, 2021), exemplifies this need. Its rivers, fed by snow, provide essential dry-

season water for irrigation, drinking, and hydropower. Despite its ecological significance, the basin's cryospheric behavior remains poorly documented.

Findings from studies conducted in the central and eastern Himalayas, the Indian Himalayas, and the Tibetan Plateau cannot be universally applied to the Karnali Basin due to differences in climatic regimes and geographical settings. Understanding the impacts of cryosphere changes on water resources requires studies specific to the Karnali Basin. Integrating MODIS data, which offers high temporal resolution, with Landsat data, known for high spatial resolution, will improve our understanding of snow and glacier changes and their relationships with topography, glacier basins, and climate.

Against this backdrop, the specific objectives of these study are to:

1. Quantify spatial and temporal variations in snow and glacier cover in the Upper Karnali Basin (2000–2024) using multi-sensor remote-sensing datasets.
2. To determine the influence of climatic drivers (rising temperatures, precipitation shifts) and topography on the observed cryospheric dynamics, including the upward migration of the snowline.

## 2. Study Area

The Upper Karnali Basin (UKB) is a transboundary catchment extending from 28.64° to 30.68° N latitude and 80.64° to 83.54° E longitude, covering 22,577 km². This region accounts for over 50% of the entire Karnali Basin above the Chisapani gauge station (225 m above sea level). It includes about 66% of the basin's glacierized area (Bajracharya et al., 2011; Ghimire et al., 2024). The UKB comprises the Humla Karnali (partly within Tibet, China), Mugu Karnali, Kawari, and Tila Nadi sub-basins (see Fig. 1).

The elevation ranges from 340 meters to 7,030 meters, with an alpine zone above 4,000 meters extending across the Middle Mountains, High Mountains, High Himalaya, and the Tibetan Plateau. These regions encompass the geological units known as the Lesser Himalaya, Higher Himalaya, and Tethys Himalaya (LRMP 1986; Dhital 2015). This topographic and lithologic diversity significantly influences climatic gradients and cryospheric processes.

The climate ranges from polar tundra in the glacier region to subtropical, temperate, and cold climates below 4,000 meters, with mean annual temperatures ranging from 27 °C to -12 °C and precipitation varying from 250 mm in rain-shadow areas to approximately 1,900 mm annually on slopes. The cryosphere spans across both rainy and rain-shadow areas, which influences the distribution and mass balance of snow and glaciers.

The Upper Karnali Basin features a diverse landscape of snow-covered glaciers, valleys, permafrost, alpine meadows, and forests, supporting a rich variety of flora and fauna. It represents a cultural blend of Khas and Tibetan traditions and is an emerging tourist destination, including a stop on the Kailash Mansarovar pilgrimage route. The basin has an estimated population of approximately 816,941 people, with a density of 36.2 persons per square kilometer, residing in 4,395 settlements, primarily below 4,000 meters in elevation. The Human Development Index in the area is 0.49, which is below the national average.

Due to its climatic, geological, and cryospheric diversity, the Upper Karnali Basin represents the broader Himalayan environment. It serves as an ideal natural laboratory for studying spatial variations in snow- and glacier-covered areas, elevation-dependent warming, and hydro-cryospheric changes across far and mid-western Nepal.

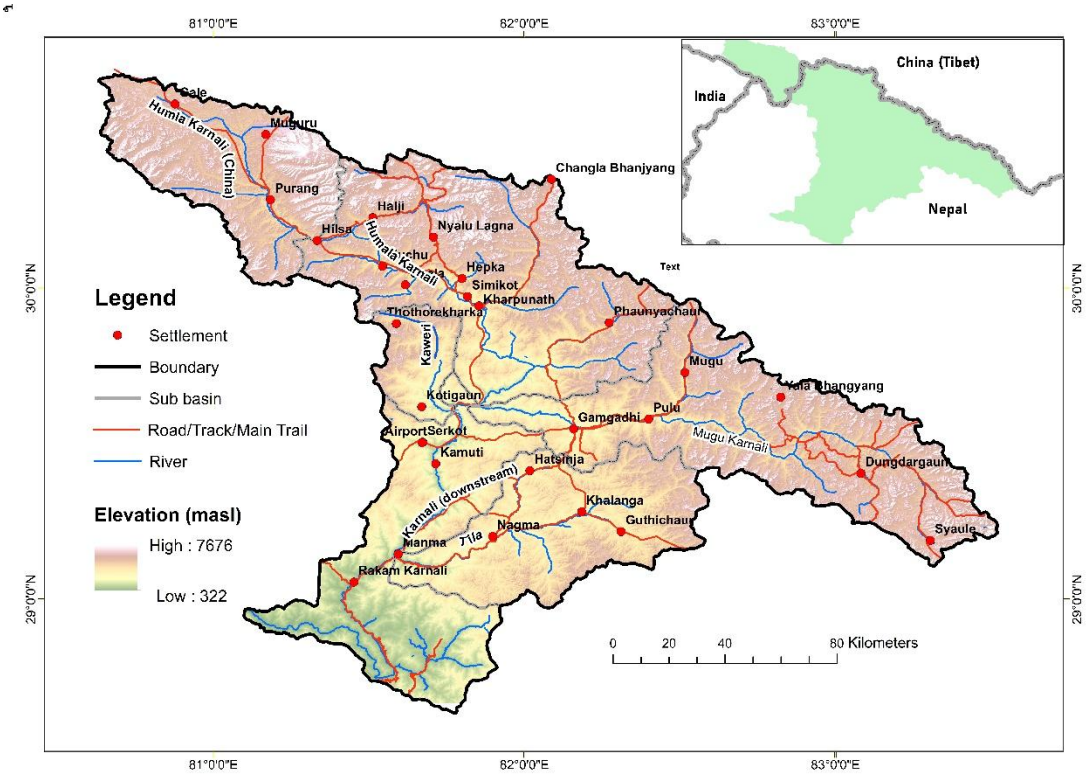


**Figure 1.** Location of the Upper Karnali Basin.

## 3. Data Sources, Method, and Limitations

This study considers snow and glacier cover as a unified cryospheric component, given their analogous functional roles. This study analyzed cryospheric dynamics using remote sensing. Satellite imagery was processed to generate time-series data on snow and ice cover, derive land-surface temperatures, and map glacier basins.

### 3.1.Snow Cover Mapping

We mapped snow cover in the Upper Karnali Basin using Google Earth Engine (GEE) and imagery from Landsat 5 TM, Landsat 7 ETM+, and Landsat 8 OLI. For the period preceding the Scan Line Corrector (SLC) failure, we used only Landsat 7 ETM+ images (2002–2003). For subsequent years, we utilized data from Landsat 5 TM and Landsat 8 OLI. To ensure high data quality, we selected only scenes with less than 30% cloud cover (Appendx A)

We preprocessed all Landsat images by masking clouds using the Quality Assessment (QA) bands–pixel_qa for Landsat 5 and 7, and QA_PIXEL for Landsat 8. Next, we calculated the Normalized Difference Snow Index (NDSI) using the green and short-wave infrared (SWIR) bands (Hall et al., 2002; Gorelick et al., 2017) and applied a threshold of NDSI > 0.4 to identify snow pixels. To reduce confusion between snow and vegetation in mixed or forested terrain, we also calculated the Normalized Difference Vegetation Index (NDVI) and excluded pixels with NDVI > 0.2 from the snow classification, following the approach of Rittger et al. (2013). Finally, we exported the resulting snow cover maps as GeoTIFF files for overlay and sub basin and micro-basin analyses.

To supplement the Landsat observations, we processed MODIS 8-day composite snow-cover products (MOD10A2) using Google Earth Engine (GEE). The MOD10A2 algorithm applies a maximum snow-extent compositing method over each 8-day period (Parajka and Blöschl, 2008), which minimizes cloud contamination and produces a spatially continuous dataset for analyzing seasonal and interannual snow-cover variability. Although it loses daily temporal resolution, the

8-day composite effectively smooths out short-lived cloud effects, providing a more stable dataset for trend analysis.

After processing the imagery, we executed a Python script within the Google Earth Engine (GEE) environment to automate the download and organization of snow cover data. The script aggregated MODIS-derived snow extent by season, sub-basin, and elevation band (derived from the SRTM DEM).

The year was divided into four distinct three-month periods—January–March (Peak Accumulation), April–June (Major Ablation), July–September (Monsoon Ablation), and October–December (Early Accumulation). This division was explicitly chosen to capture the hydrological phases of snow accumulation and melting while minimizing cloud contamination during the monsoon season(Hunt et al., 2025; Khatiwada et al., 2016; Kulkarni et al., 2017). The resulting structured snow dataset was used as the main input for analyzing snow cover trends, elevation-dependent variability, and hydrological differences among sub-basins.

We describe the methods for spatial resolution harmonization and accuracy assessment between Landsat and MODIS datasets in Appendix B. Despite these refinements, persistent monsoon cloud cover continues to limit optical remote sensing in the Himalayas, often resulting in underestimation of snow-covered areas and uncertainties in seasonal trends.

Elevation bands were defined using the SRTM DEM and categorized into 200-meter intervals, ranging from ≤2000 m to ≥6500 m. Zonal statistics were applied to extract the frequency of snow cover for each elevation band and subbasin. Snow-covered area was calculated using a threshold-based binary mask. The results were aggregated into a structured dataset, revealing

seasonal snow distribution and variations across elevation zones and watersheds, thereby facilitating hydrological analysis.

### 3.2. Land Surface Temperature Data and Validation

We also downloaded the land surface temperature (LST) 1 km resolution from the Application for Extracting and Exploring Analysis Ready Sample (AppEEARS) platform. AppEEARS is a NASA-supported platform developed to easily access, subset into specified areas, and analyze climate and environmental data(Wan et al., 2015). MODIS Land Surface Temperature (LST) data have been reliably used to determine surface temperature patterns in areas where ground observations are scarce, especially in rugged mountainous regions. Several studies have confirmed their accuracy, showing average biases of less than 1.5 K and high correlations ($R^2 >$ 0.9) with on-site measurements (Duan et al., 2019; Yu et al., 2011; Zhao et al., 2019), demonstrating their appropriateness for analyzing elevation-related warming trends in the Himalayas. We also obtained temperature and precipitation records, including maximum and minimum values, from the Department of Hydrology and Meteorology (DHM), Government of Nepal, and open-access reanalysis datasets such as ERA5. The temperature data (2 m above ground) obtained from various meteorological stations in the study area, were compared with MODIS LST; the results of this comparison are discussed in Section 4. Due to the 1 km spatial resolution of the MODIS product, the analysis of time series data reflects area-averaged temperature trends rather than in situ measurements at individual stations.

### 3.3. Delineation of the Glacier Basin and Glacier Data

The boundaries of glacier basins were delineated to assess changes in glaciers and snow cover fractions within glacier-drained areas. Glacier basins include trunk glaciers, tributary glaciers,

and surrounding slopes nourished by moving ice and snow. Their boundaries are topographically defined, with the lower boundary terminating at the terminus of the main glacier. This delineation process involved multiple steps to ensure accuracy.

Initially, the Glacier Inventory map referenced earlier served as a fundamental resource. High-resolution imagery and ESRI's topographic maps in ArcGIS 10 and later versions provided detailed spatial data. A 12.5 meter DEM was used to extract drainage networks, produce contour lines, and generate hillshade maps, enhancing the visualization of divides between glacier basins. These components were essential for accurately identifying glacier termini and delineating glacier head basins. This integrated approach, combining topographic analysis, remote sensing, and geospatial techniques, enabled precise delineation of glacier basins for comprehensive evaluations of snow cover fraction.

The time series glacier data compiled by Ghimire et al. (2025), were included in this study. The lead author of the current manuscript was also responsible for that research paper. In summary, we mapped glacier polygons for the years 2000, 2010, and 2023 using high-resolution imagery from Google Earth, Bing Maps, and RapidEye 2023 to maintain temporal consistency. Snow and glaciers were identified based on their bright characteristics, features, smooth textures, and shadows cast by adjacent terrain. Landsat composites (both true and false color) and the Normalized Difference Snow Index (NDSI) enhanced and improved the visibility of snow and ice, while altitude and topographic data derived DEM highlighted potential glacier regions. Outlines from the Randolph Glacier (RGI)(Pfeffer et al., 2014) and ICIMOD (Bajracharya et al.) served as reference, while ground-truth and additional data helped validate the findings. This comprehensive approach ensured precise delineation.

### 3.4.Limitations and Validation

A key limitation of this research is that optical remote sensing is significantly affected by cloud cover, particularly during the monsoon season (Hall et al., 2002; Gafurov and Bárdossy, 2009). Frequent cloudiness often restricts the availability of clear Landsat images, leading to an underestimation of snow cover and potential inaccuracies in the spatial and seasonal assessment of snow patterns. In this study, cloud-free images were primarily available from January to March and October to December in most Upper Karnali sub-basins. Nevertheless, all four seasons were analyzed for microglacier basins where suitable data existed.

To address these issues, we used MODIS MOD10A2 data, which provide higher temporal resolution (8-day composites at 500 m) compared to Landsat's 16-day revisit cycle and 30 m spatial resolution. This multi-sensor strategy enhances temporal continuity and minimizes data gaps caused by clouds; however, results should still be interpreted cautiously (Maskey et al., 2011; Parajka and Blöschl, 2008).

The scarcity of high-altitude temperature stations necessitated the use of MODIS land surface temperature (LST) data at a 1 km resolution, representing daytime skin temperature at approximately 10:30 A.M. local time. This skin temperature was compared with in situ air temperature measurements taken at 2 meters above ground from four stations: Jumla (2,300 m), Simkot (2,800 m), Guthi Chaur (3,080 m), and Rara (3,048 m). Correlations varied by site and season–strongest at Jumla (up to 0.85), moderate at Guthi Chaur, and weakest at high-altitude, snow-covered sites such as Simkot and Rara (−0.18). MODIS LST performs well in clear, snow-free areas but requires adjustments at higher elevations. Differences arise from factors including resolution, spatial averaging, land-cover heterogeneity, and surface–air temperature contrasts. Validation studies further confirm its reliability for analyzing high-mountain temperatures in regions where in situ data are limited (see Duan et al., 2019; Yu et al., 2011; Zhao et al., 2019).

## 4. Result

### 4.1. Snow or Ice cover Trend and Variability: Annual and Seasonal

The total snow cover across the Upper Karnali Basin (22,546 km²) from 2002–2024 averages 872 km², with a standard deviation of 147 km², indicating moderate variability (Table 1 and Figure 2 ). The minimum recorded snow cover is 514 km²; about 25% of the recorded snow cover observations are at or below 777 km². The average snow covered area from January–March is 1528 ±333 $km^2$, followed by April-June (881 ± 212 $km^2$) and October–December (862±373 $km^2$), respectively. July–September witnessed the lowest snow cover area, i.e., 169 ±38.3 $km^2$ .

Snow cover data highlight significant year-to-year changes in every quarterly season with varying directions and magnitudes of trends, evidenced by correlation, the Kendall tau test, and Sen's slope. The annual average SCA shows, although not significant, a decreasing trend (p = 0.535), with Sen's Slope estimating a loss of ~3.99 $km^2$/year, which indicates a gradual decline in snowpack over two decades. Seasonally, the July–September period exhibits a gentler trend line compared to October–December; however, because of its much lower inter-annual variability, this period exhibits the statistically significant steepest drop in snow cover (Sen's Slope = -2.87, p = 0.001) (Table 1). This period is charactersied by snow ablation, where the summer monsoon brings warmer temperatures. In mid-latitude regions, the precipitation occurs more as rain than snow, resulting in accelerated snowmelt. While January–March shows a decline (Sen's slope =-8.63 km/year), it lacks statistical significance (p = 0.523), suggesting year-to-year winter variability in snowfall or early melt. Similarly, no significant trends were detected in April–June. Interannual variability is evident with peaks and lows of snow and ice coverage (Figure 2). Episodic snow coverage was observed in 2015, 2020, and 2022 (January–March), 2015 and 2019

(April–June), 2009, and 2021 (October–December), indicating anomolous years of high episodic heavy snowfall events. However, these anomalies do not counterbalance long-term declines. Compared to seasons, annual snow coverage's inter-annual variability is relatively low, i.e., with a 16% coefficient of variation (CoV)–ratio of the standard deviation to the mean.

**Table 1**. Snow cover descriptors and changes by seasons

| **Descriptor** | **Jan–Mar** | **Apr–Jun** | **Jul–Sep** | **Oct–Dec** | **Annual avg.** |
|---|---|---|---|---|---|
| Mean (km²) | 1 528.00 | 881.00 | 217.00 | 862.00 | 872.00 |
| Median (km²) | 1 569.00 | 858.00 | 210.00 | 739.00 | 886.00 |
| Std. dev. (km²) | 333.00 | 212.00 | 38.30 | 373.00 | 147.00 |
| Minimum (km²) | 1 025.00 | 503.00 | 169.00 | 340.00 | 514.00 |
| Maximum (km²) | 2 167.00 | 1 358.00 | 298.00 | 1 737.00 | 1 055.00 |
| Skewness | 0.21 | 0.47 | 0.94 | 0.51 | −0.87 |
| 25th percentile (km²) | 1 270.00 | 751.00 | 191.00 | 538.00 | 777.00 |
| 50th percentile (km²) | 1 569.00 | 858.00 | 210.00 | 739.00 | 886.00 |
| 75th percentile (km²) | 1 689.00 | 1 025.00 | 229.00 | 1 126.00 | 991.00 |
| Correlation (r) | −0.09 | −0.07 | −0.61 | −0.25 | −0.27 |
| Kendall's τ | −0.09 | 0.01 | −0.54 | −0.13 | −0.10 |
| p-value | 0.523 | 0.950 | 0.000 | 0.398 | 0.535 |
| Sen's slope (km² $yr^{-1}$) | −8.63 | −3.14 | −2.87 | −13.21 | −3.99 |

**Note:** Sen's slope represents the median of all possible pairwise slopes, quantifying trend (here snow cover) over time (Sen, 1968). It gives a more reliable long-term trend of snow cover loss without being skewed by short-term anomalies (Gilbert, 1987; Yue and Wang, 2004)

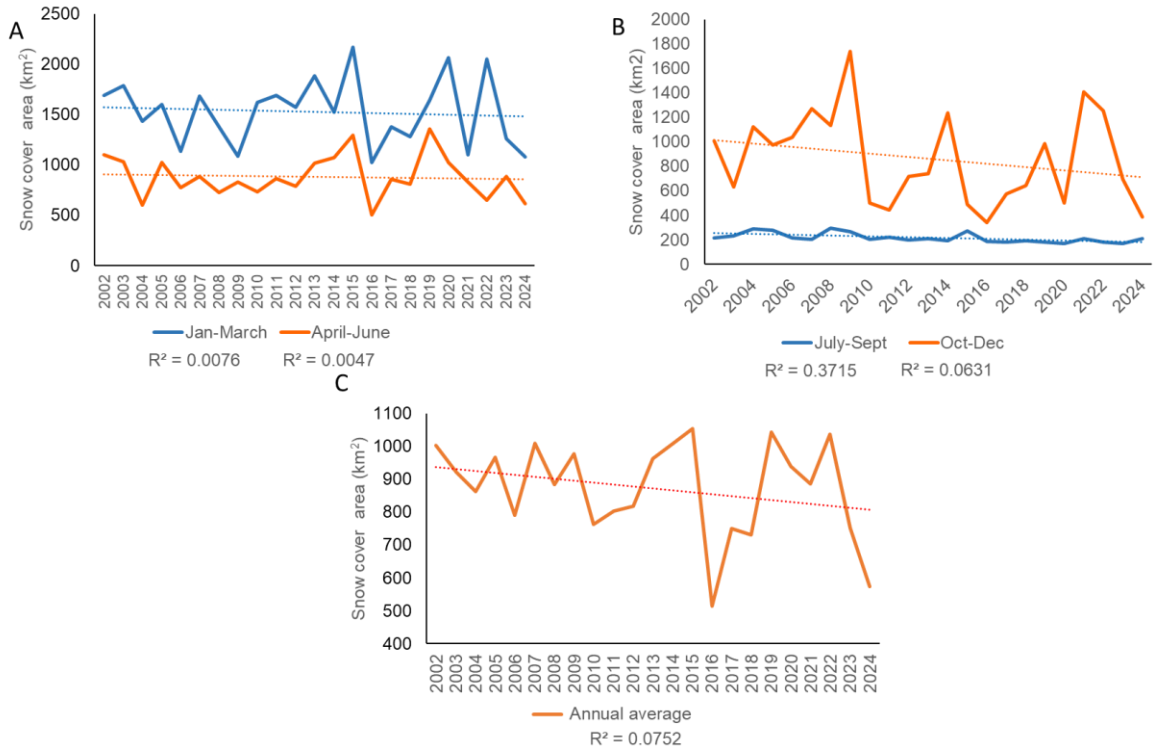


280

281

282 **Figure 2.** Temporal variation and trends in seasonal and annual snow-covered area (SCA) in the
283 Upper Karnali Basin (2002–2024).a) Time series of SCA for January–March (orange) and April–
284 June (orange); (b) SCA for July–September (blue) and October–December (orange); (c) average
285 annual SCA (orange).

286 ### 4.2. The Relation among Snow Cover, Temperature, and Precipitation

287 We derived land surface temperature (LST) data for 204 locations from MODIS Terra
288 (MOD11A1) and Aqua (MYD11A2) (1 km resolution), which were processed through
289 AppEEARS. Precipitation data were obtained from the ERA5-Land reanalysis (~9 km
290 resolution) by ECMWF (Hersbach et al., 2020). These datasets, covering four different seasons,
291 were used to examine temperature and precipitation trends, as well as their relationship with
292 snow cover trends (Figures 3, 4, and 5).

Using correlation statistics, we found that among the 204 sampled sites, 143 locations (approximately 70%) exhibit a positive annual temperature trend, indicating a general warming pattern throughout the study region (Figure 3). However, statistically significant trends ($p \leq 0.1$) were identified in only a subset of these sites, highlighting that not all observed warming trends are statistically robust. Moreover, the warming pattern is not consistent across all seasons. Notably, during the April–June interval, the temperature trend tends to be weaker or, in some cases, negative. Several subsites across different seasons also demonstrate negative trends, although the majority of locations show a positive trend (Figure 3). Elevation-related variability in these trends is further analyzed in Figures 7–9 and Table 3.

Seasonal rainfall trends from 2000 to 2024 indicate weak to moderate increases across all seasons, with the exception of winter (January–March), which exhibits a slight downward trend ($R^2$= 0.0144) (Figure 4). Pre-monsoon (April–June) rainfall shows a slight upward trend ($R^2$ = 0.0119). All these seasons display high variability, suggesting a limited impact on snow accumulation. Monsoon rainfall (July–September) demonstrates a more noticeable increase ($R^2$ = 0.0975), primarily contributing to rainfall rather than snowfall. Post-monsoon (October–December) precipitation remains low and stable. When combined with rising temperatures, these trends indicate a shift toward rainfall-dominated precipitation, reduced snowfall, and earlier snowmelt, contributing to declining snow cover and altered hydrological regimes.

The snow-covered area shows a strong to moderate negative correlation ($r = -0.59$ to $-0.77$, $p < 0.05$) with temperature across all seasons (Figure 5). Conversely, precipitation has a positive correlation ($r = 0.55$ to $0.59$, $p < 0.05$) with snow cover for January–March and October–December, while during the remaining seasons, it shows a moderate negative correlation.

316 Precipitation and temperature are negatively correlated in winter (Oct-March) and positively in
317 the summer (April-September) half-year.

318

319

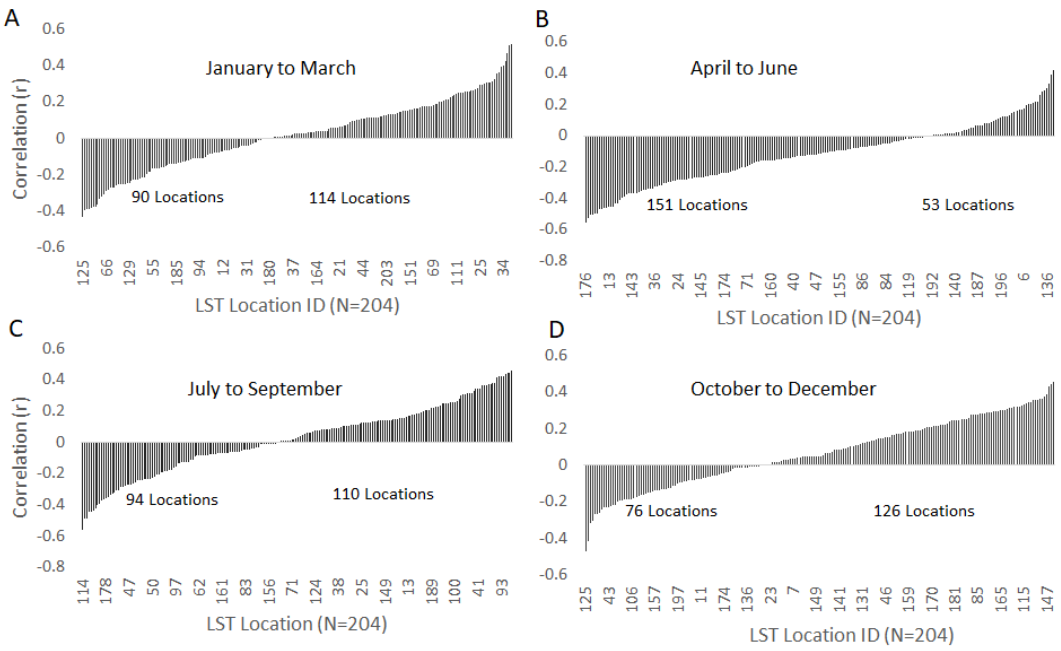


320

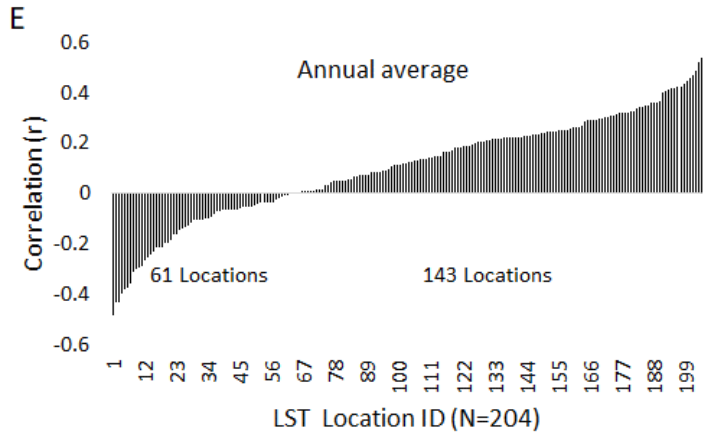


321

**Figure 3.** The correlation illustrates the season wise (A-E) temperature trend directions at various sites between 2000 and 2024 (Source: MODIS Terra and Aqua MOD11A2, MYD11A1, AppEEARS). Significant correlations at a 90 % confidence level are observed at r= ±0.364.

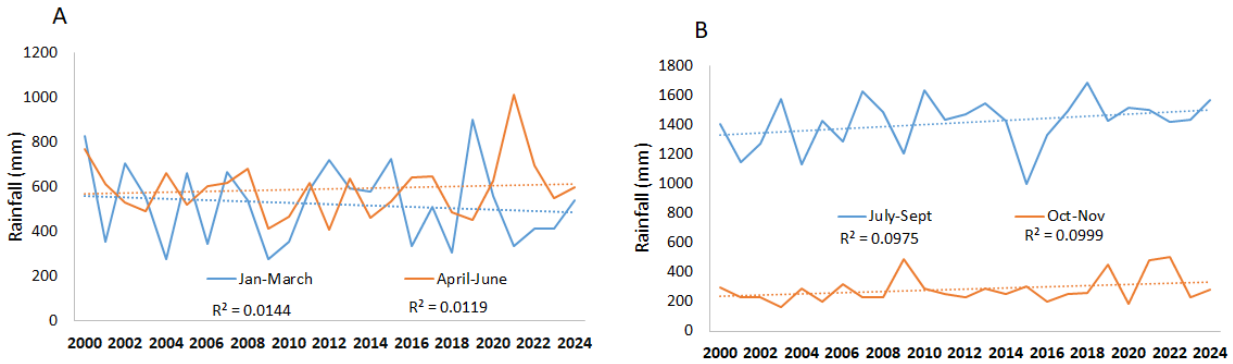


**Figure 4.** Yearly rainfall trends across various periods. Precipitation data was collected from the ERA5-Land reanalysis by ECMWF (Hersbach et al., 2020) from 204 locations across four different periods.

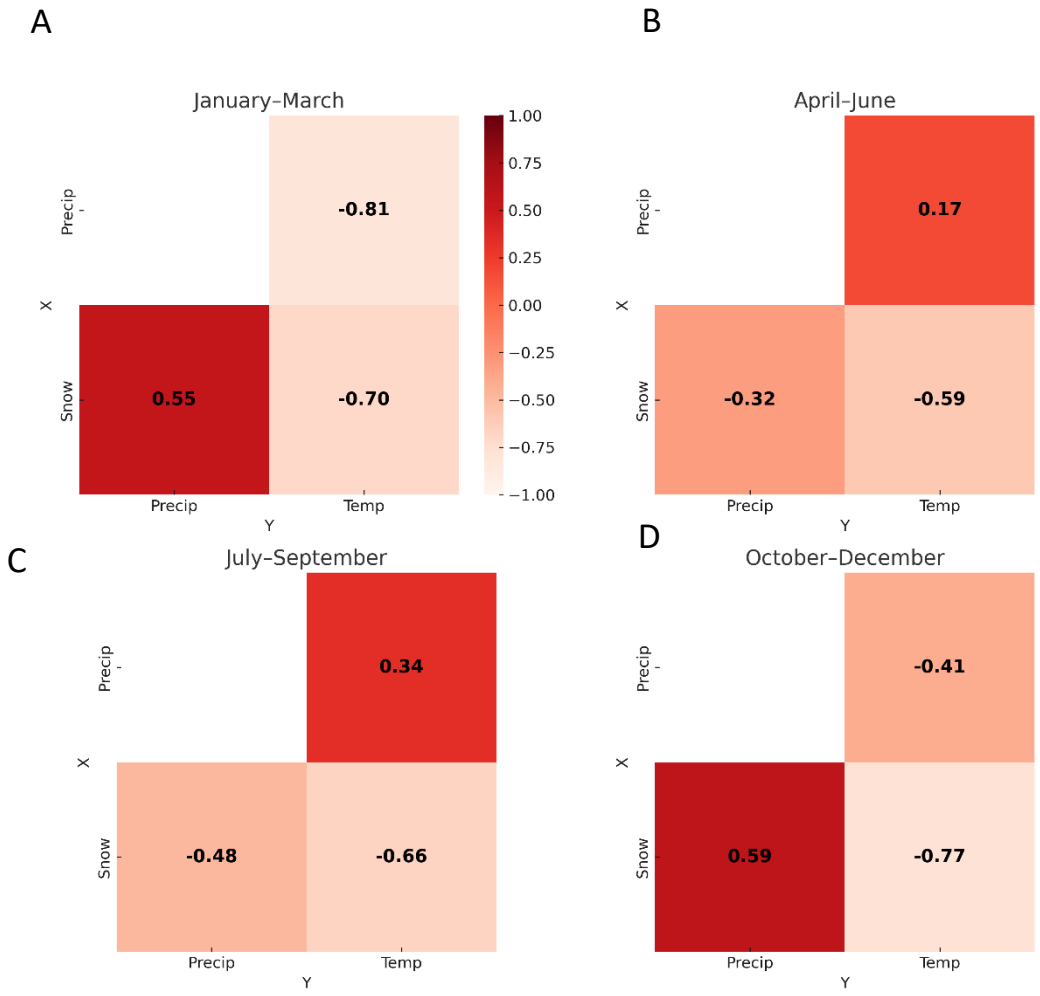


**Figure 5**. Seasonal correlation patterns among snow cover, temperature, and precipitation across a 22-year period, shown separately for each season (A–D).

### 4.3. Snow Cover Changes in Sub-Basins Using Landsat Series Data

Landsat-derived reliable snow and ice data were unavailable for the pre-monsoon and monsoon seasons due to significant cloud coverage (as mentioned in Section 3.4). Therefore, only two seasons, January–March and October–December, were considered. These seasons are characterized by snowfall as precipitation, which contributes to snow accumulation.

Examining snow cover patterns in the sub-basins of the Upper Karnali Basin (UKB) for two seasons (January–March and October–December) reveals notable seasonal and spatial

differences (Table 2). During January–March, Humla Karnali has the largest average snow cover (3,336 km²), followed by Mugu Karnali (1,864 km²) and Humla Karnali (China) (1,478 km²), while areas downstream like Tila and Kawari have very little coverage (less than 350 km²). Significant variability in the snow cover trend is observed, particularly in Tila and Downstream Karnali, which have a coefficient of variation (CoV) above 50%. This high CoV indicates inconsistent snow cover from year to year during January–March. Furthermore, this variability is associated with a significant negative correlation i.e., $r \geq -0.37$ ($p<0.1$). Figure 6 also graphically shows the temporal trends with the correlation coefficient (r) and fluctuations in Landsat-derived snow cover for the two seasons mentioned above. The moderately negative skewness of the temporal distribution does not affect the correlation, which is negative for all basins, indicating a declining trend.

Conversely, the October–December season has a lower average snow cover (823 km²) and exhibits strong fluctuations (e.g., a range of 227–1570 km² and a CoV of 55%). Strong variability is observed for all basins, particularly Humla Karnali (China), Tila, and Downstream Karnali. The skewness is moderate, except for Downstream Karnali. Correlation values are reliable and indicate a declining trend. However, Downstream Karnali, in spite of high variability, indicates a statistically significant negative r value, i.e., -0.47 ($p<0.05$) (Figure 6).

**Table 2.** Descriptive statistics of snow cover across sub-basins for two seasons (January-March and October-December) and the time series correlation from 2002 to 2024.

| Descriptor | January - March | | | | | | | October-December | | | | | | |
|---|---|---|---|---|---|---|---|---|---|---|---|---|---|---|
| | Humla Karnali (China) | Humla Karnali | Mugu Karnali | Tila | Kaweri | Down stream | Seasonal average | Humla Karnali (China ) | Humla Karnali | Mugu Karnali | Tila | Kaweri | Karnali (Down stream) | Seasonal average |
| Mean | 1478 | 3336 | 1864 | 351 | 294 | 41.9 | 1227 | 854 | 2057 | 1442 | 332 | 204 | 48.1 | 823 |
| Median | 1420 | 3667 | 1827 | 346 | 308 | 39 | 1239 | 754 | 2159 | 1301 | 288 | 190 | 40.2 | 781 |
| Standard deviation | 501 | 597 | 645 | 184 | 86.2 | 24 | 311 | 622 | 1163 | 862 | 227 | 112 | 44.7 | 457 |
| Coefficient of variation (CoV in %) | 33.90 | 17.90 | 34.60 | 52.42 | 29.32 | 57.28 | 25.35 | 72.83 | 56.54 | 59.78 | 68.37 | 54.90 | 92.93 | 55.53 |
| Minimum | 552 | 1904 | 887 | 50.1 | 121 | 5.74 | 612 | 67.2 | 166 | 226 | 44.3 | 35.2 | 3.28 | 227 |
| Maximum | 2317 | 4009 | 3056 | 691 | 420 | 93.5 | 1642 | 2092 | 4074 | 2868 | 716 | 434 | 185 | 1570 |
| Skewness | -0.707 | -0.488 | -1.29 | -0.69 | -0.469 | -0.763 | -1.1 | 0.533 | -0.016 | 0.231 | 0.347 | 0.204 | 1.43 | 0.202 |
| Temporal correlation (r<-0.44 and r>0.44, p<0.05 | -0.16 | -0.18 | -0.10 | 0.12 | -0.37 | -0.41 | -0.14 | -0.16 | -0.07 | -0.23 | -0.17 | -0.13 | -0.47 | -0.17 |

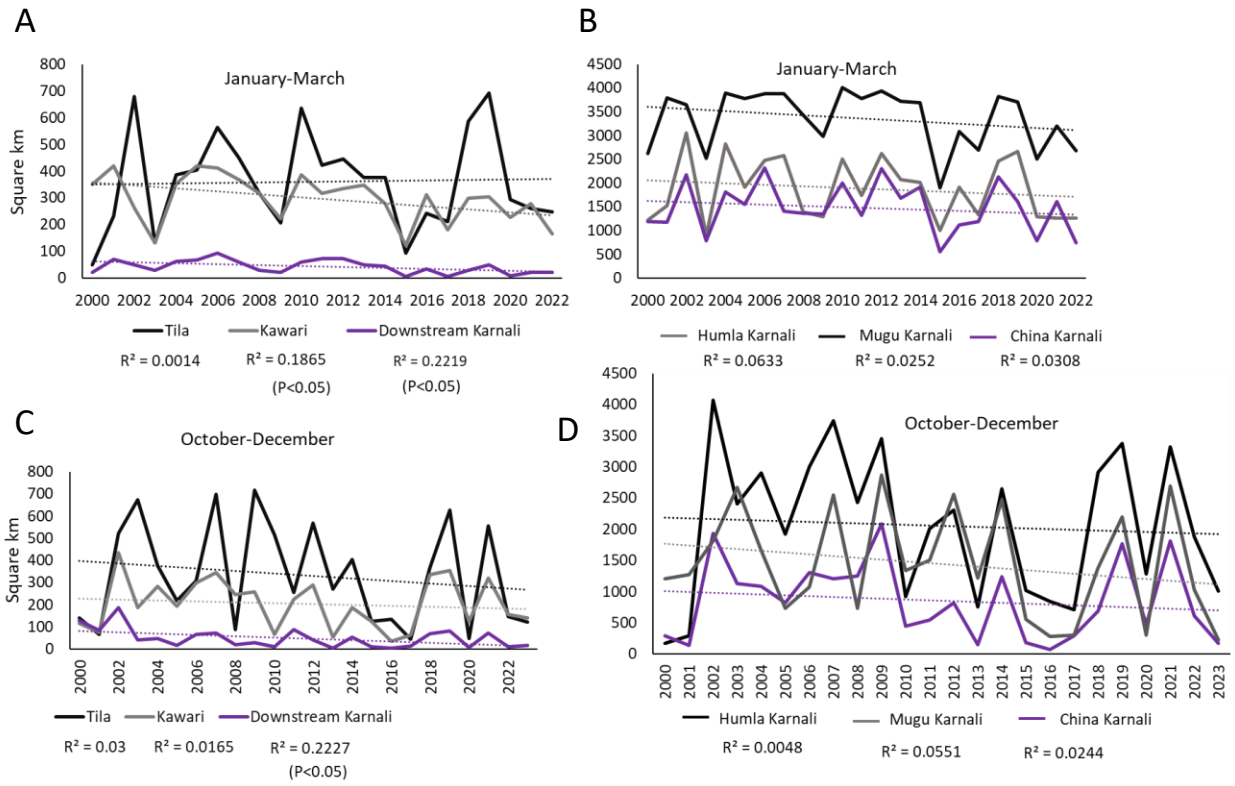


**Figure 6.** The snow cover trend in the Upper Karnali Basin varies across different sub-basins from January–March and from October–December (A-D).

### 4.4. Snow Cover Dynamics across Elevation Zones

The dynamics of snow cover across elevation zones, categorized in 200-meter intervals from ≤2000 m to ≥6500 m, reveal remarkable elevation-dependent patterns in correlation and variability (Figure 7) with time (2002-2024). Snow cover in the lowest elevation zones shows a weak positive correlation (0.12-0.43), suggesting a marginal increase. However, pronounced

interannual variability (CoV ~ 41-43%) is likely driven by fluctuating temperature and precipitation regimes (Pendergrass, 2020).

Above 2300 m a.s.l., correlations shift to weak negative values (up to 5000 m a.s.l., r = -0.05 to -0.17, reaching peak negativity at 6100-6200 m a.s.l. (r = -0.56), indicating a significant decline in snow cover (Figure 7). This trend aligns with the impacts of global warming, where rising temperatures disproportionately affect higher elevations, accelerating snowmelt and reducing accumulation (Naegeli et al., 2019; Ren et al., 2023; Shen et al., 2021). The mean snow cover increases with elevation, showing a marked rise from 3300 to 6500 m a.s.l. or above, except between 5000-5200 m a.s.l, which exhibits a gradual rise in snow cover.

Above this elevation, the mean snow cover area rises sharply, coinciding with glaciers and permanent snow zones. In contrast, the CoV increases with elevation up to 3100 m a.s.l. and then trends sharply downward from 3100 m a.s.l. to 6500 m a.s.l. and beyond. This pattern indicates a decline in interannual variability alongside increased negative correlations. The low inter-variability reinforces the reliability of the declining trend in snow cover.

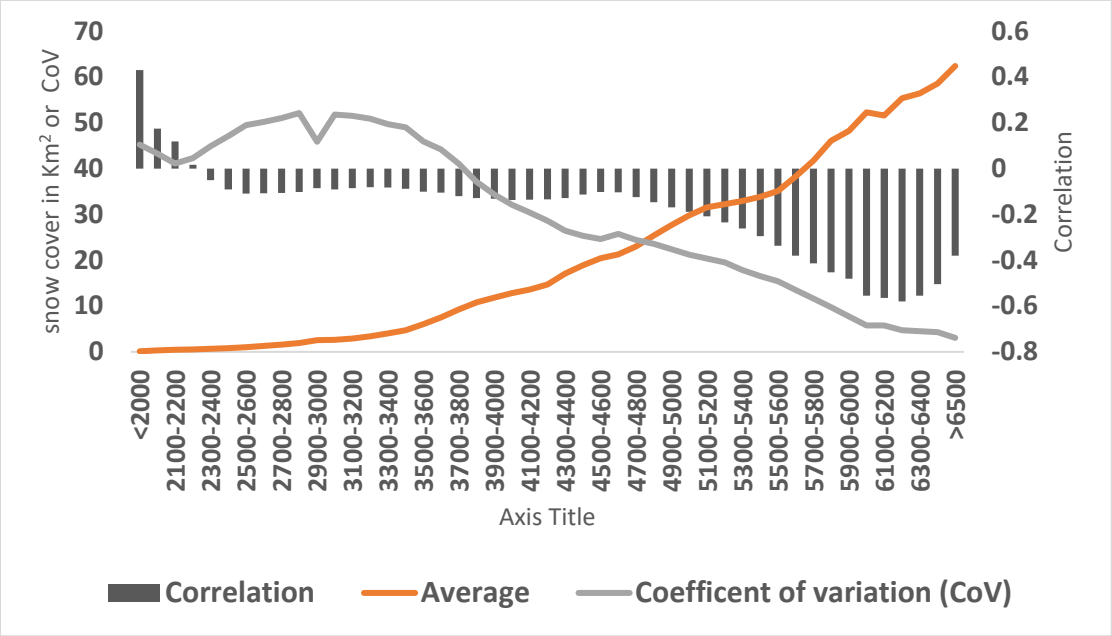


386

387 **Figure 7.** The average, coefficient of variation, and correlation of snow cover area (Source :
388 MODIS) across various elevation bands with time (2002-2024).

389 To examine the relation between temperature and snow cover, the elevation bands were
390 regrouped into seven broader bands: <1000, 1000–2000, 2000–3000, 3000–4000, 4000–5000,
391 5000–5500, 5500–6000, and above 6000 m a.s.l. The temperature trend from 2002 to 2024
392 across elevation bands in the Upper Karnali Basin, as evidenced by Sen's slope (Figure 8, Table
393 3), shows a general increase. The highest rate of change is observed at lower elevations (<1000
394 m: 0.0765°C/year). Mid-elevations (1000-2000m: 0.0576°C/year) and high elevations (5000–
395 5500 m: 0.0643°C/year) also exhibit significant warming. However, statistical significance (P-
396 value) weakens at higher elevations. This warming accelerates glacier retreat, reducing snow
397 cover and impacting the hydrology of the Upper Karnali Basin by altering river flow patterns and
398 leading to a declining glacier-fed water supply.

399

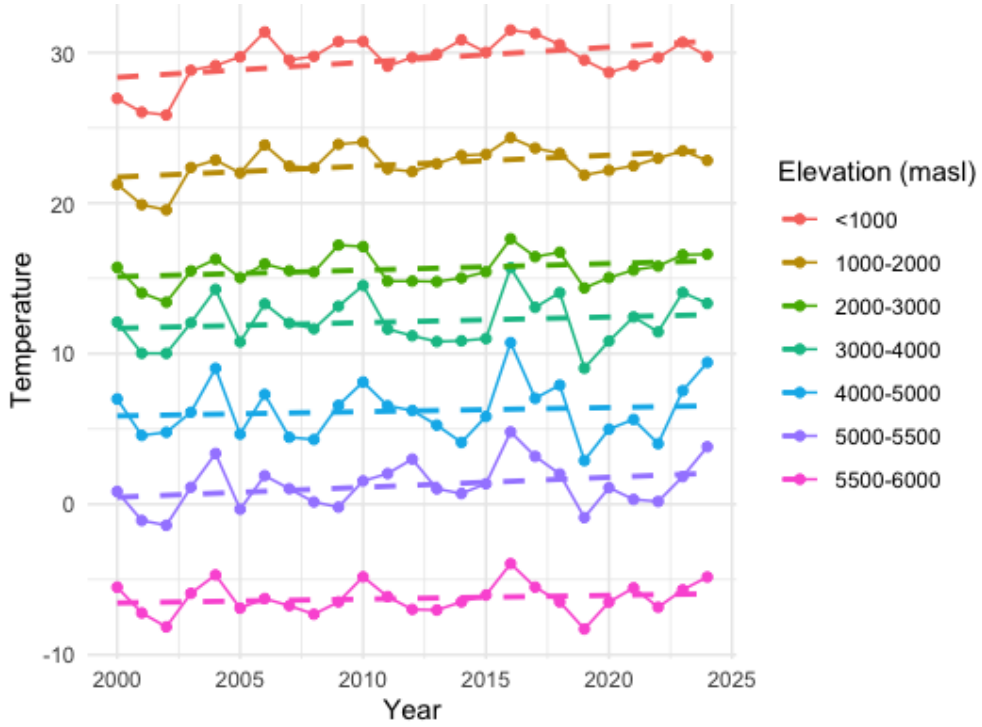


400

401 **Figure 8.** Temperature (source: MODIS) trend between 2002 and 2024 for different elevation

402 bands

403

**Table 3.** Rate of temperature change in different elevation between 2000–2024)

| Elevation bands (m a.s.l.) | Sen's slope(Sen, 1968) | P Value |
|---|---|---|
| <1000 | 0.0765 | 0.052 |
| 1000–2000 | 0.0576 | 0.058 |
| 2000–3000 | 0.0390 | 0.168 |
| 3000–4000 | 0.0410 | 0.528 |
| 4000–5000 | 0.0198 | 0.833 |
| 5000–5500 | 0.0643 | 0.154 |
| 5500–6000 | 0.0287 | 0.414 |

Figure 9 shows a strong negative correlation between land surface temperature and snow cover across elevation bands in the Upper Karnali Basin. Tau values range from -0.43 to -0.79. The correlation is strongest between 3000–5000 m a.s.l. (Tau = -0.77 to -0.79) and 5000–5500 m a.s.l. (Tau = -0.75), with all p-values <0.01, confirming statistical significance. Even at 5500–6000 m a.s.l. (Tau = -0.43, p = 0.00353), snow cover continues to decline. The impact is most severe at mid-to-high elevations, where warming accelerates snowmelt and glacier retreat, highlighting the vulnerability of the Upper Karnali Basin's hydrological balance to climate change.

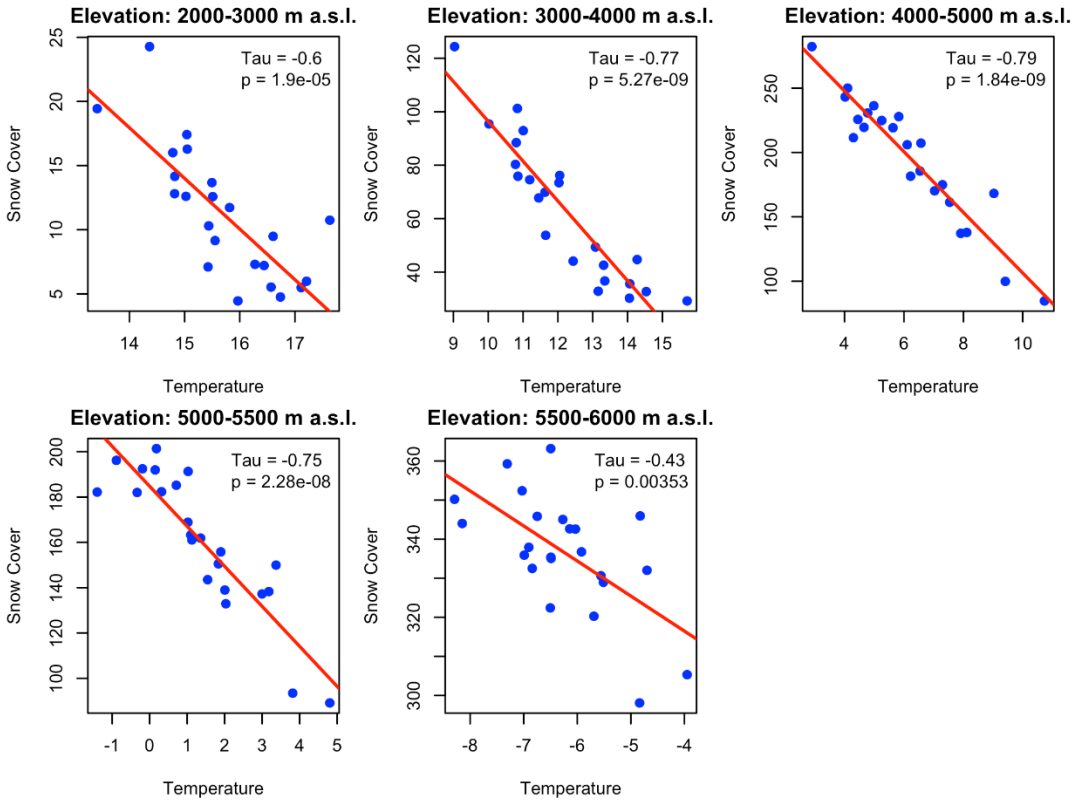


414

415 **Figure 9.** Relationship between snow cover and temperature (°C) across elevation zones in the
416 Upper Karnali Basin (2002–2024). The correlation (Kendall's Tau) shows a strong negative
417 association across all elevations, especially between 3000–5500 m a.s.l., where warming has
418 significantly reduced snow cover.

419 **Note:** Elevation bands below 2000 m are excluded due to minimal snow presence, high
420 interannual variability, and limited data reliability.

421 **4.5. Snow Cover Trend in Glacier Basins (Landsat Data).**

422 We examined using Landsat data snow cover trends in 735 glacier basins, each containing at
423 least one glacier in 2000 that was greater than 10 hectares, which are crucial for assessing glacial
424 status, water security, and climate change impacts (Table 4). The minimum altitude of the glacier
425 basin where all tributary glaciers meet was considered the outlet of the glacier basin. In these
426 basins, snowfall restocks ice lost to melting, contributing to glacier stability. Reduced snow

cover in the glacier basins accelerates negative mass balance, leading to glacier retreat. These glacier basins are at a minimum altitude above 4000 m a.s.l. with an average of ~5100 m a.s.l. Twenty-five and 75 % lie below 4800 and 5330 m a.s.l., respectively. Besides other meteorological parameters, current temperature trends and albedo patterns play a critical role in glacier mass balance (Dowson et al., 2020; Ye & Tian, 2022). Higher temperatures directly increase the snow melting rate, and a decrease in reflectivity of solar radiation leads to more solar radiation being absorbed by the glacier surface, leading to accelerated melting. Declining permanent snow cover in the glacier basin disrupts the glacier mass balance, affecting glacier persistence, altering water availability, and accentuating climate-driven environmental changes.

The data reveal a significant decline in glacier area across 735 glacier basins between 2000 and 2023. The mean glacier area decreased from 119.0 ha in 2000 to 100.5 ha in 2023, reflecting an average loss of 18.6 ha per basin. The total glacier area shrank by 13,633.2 ha, indicating widespread glacier retreat. The percent of glacier area to total basin area declined from 53.23% in 2000 to 44.93% in 2023. Statistical tests show high skewness (>3.9), suggesting that a few large glaciers dominate the dataset. The Shapiro-Wilk test ($p < .001$) confirms a non-normal distribution.

**Table 4.** Change in glacier area between 2000 and 2023.

| Glacier basin count (N=735) | Glacier basin Area (hectares) | Glacier area (hectares) | | Difference in glacier area (hectares) |
|---|---|---|---|---|
| | | 2000 | 2023 | |
| Median | 101.4 | 52.8 | 39.7 | -10.0 |
| Mean | 223.6 | 119.0 | 100.5 | -18.6 |
| Std. Dev | 368.1 | 187.1 | 169.9 | 27.2 |

| | | | | |
|---|---|---|---|---|
| Skewness | 4.6 | 4.0 | 4.0 | -4.0 |
| Sum | 164140.9 | 87379.9 | 73746.8 | -13633.2 |

The glacier area has declined significantly across all basin directions from 2000 to 2023, with the basins oriented toward North, Northwest, and Northeast experiencing the largest losses, totaling 6,126.9 hectares (Figure 10). The glaciers oriented towards North-east, East, and South slopes show the highest relative loss (%). The consistent loss across all directions highlights the ongoing effects of climate change on the region's glacier-fed water resources.

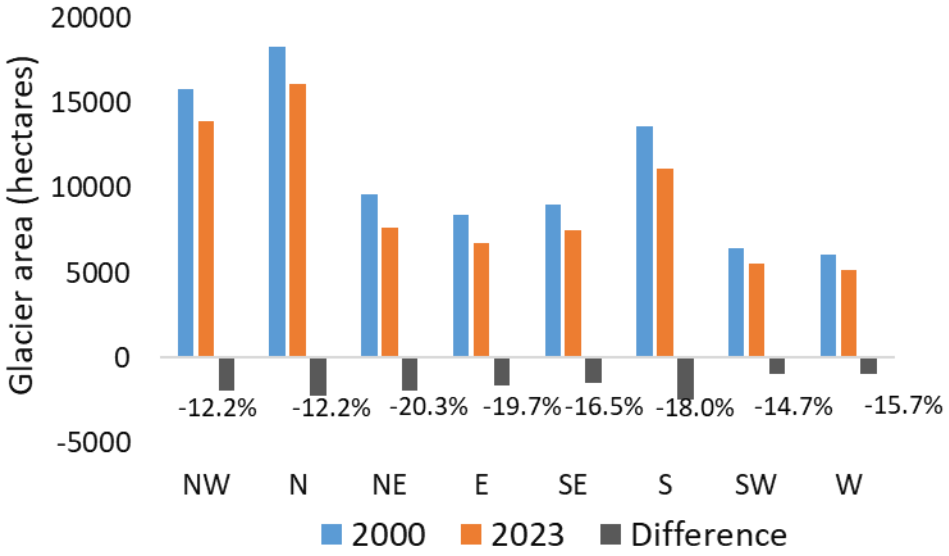


**Figure 10.** Change in glacier area in glacier basins by directions between 2000 and 2023.

Analysis of snow cover trends indicates that around 59% of glacier basins (n=735) demonstrate statistically significant negative correlations ($p<0.05$) from January to March. Among these, glacier basins with a correlation (r) value less than -0.44 represent 16.3% of the total (Figure 11, 12, and 13). Basins with moderate negative correlations, ranging from -0.44 to -0.30, constitute approximately 19% of the overall total. Additionally, 36% of basins show a positive correlation,

with 3% being statistically significant and 13% displaying a moderate correlation. The numerous glacier basins that exhibit negative correlations suggest a broader regional trend of declining snow cover over time during winter (January to March).

Similarly, during May–July, all 15 cloud-free glacier basins demonstrate a declining trend in snow cover from 2002 to 2024. Twelve of these basins exhibit a moderate negative correlation ($r < -0.30$). The trend in snow cover during July–September and October–December also indicates a decline. Sixty two percent of the 70 glacier basins show a statistically significant negative correlation ($p<0.05$)

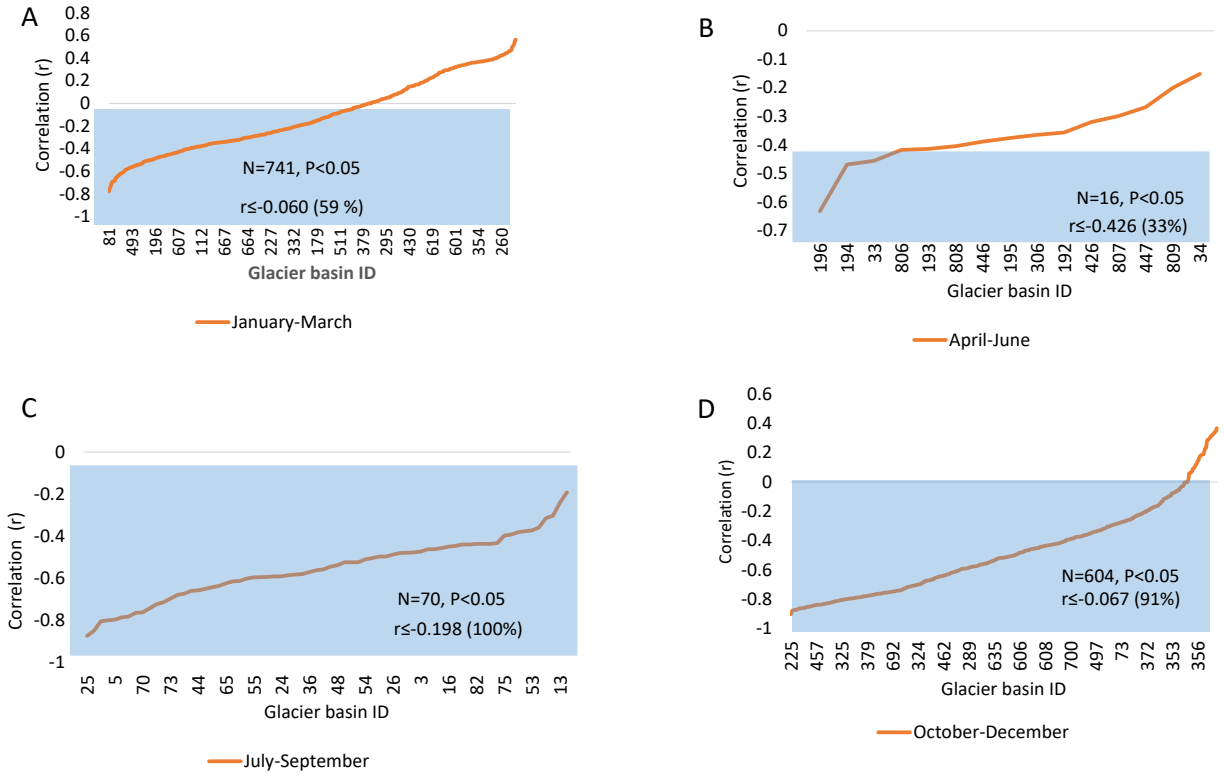

**Figure 11.** The correlation showing the snow cover change between 2002 and 2024 in different glacier basins.

The snow cover trend between July–September and October–December for 22 years also demonstrated a consistent decline in all glacier basins. Out of 604 basins selected for the analysis, about 91% have shown a statistically significant negative correlation ($p<0.05$), and 15 % of glacier basins showed a moderate negative correlation, i.e., r= -0.47 to -0.30 (Figure 10). The snow cover in the remaining basins exhibits a poor negative correlation yet indicates a decline in snow cover over the period.

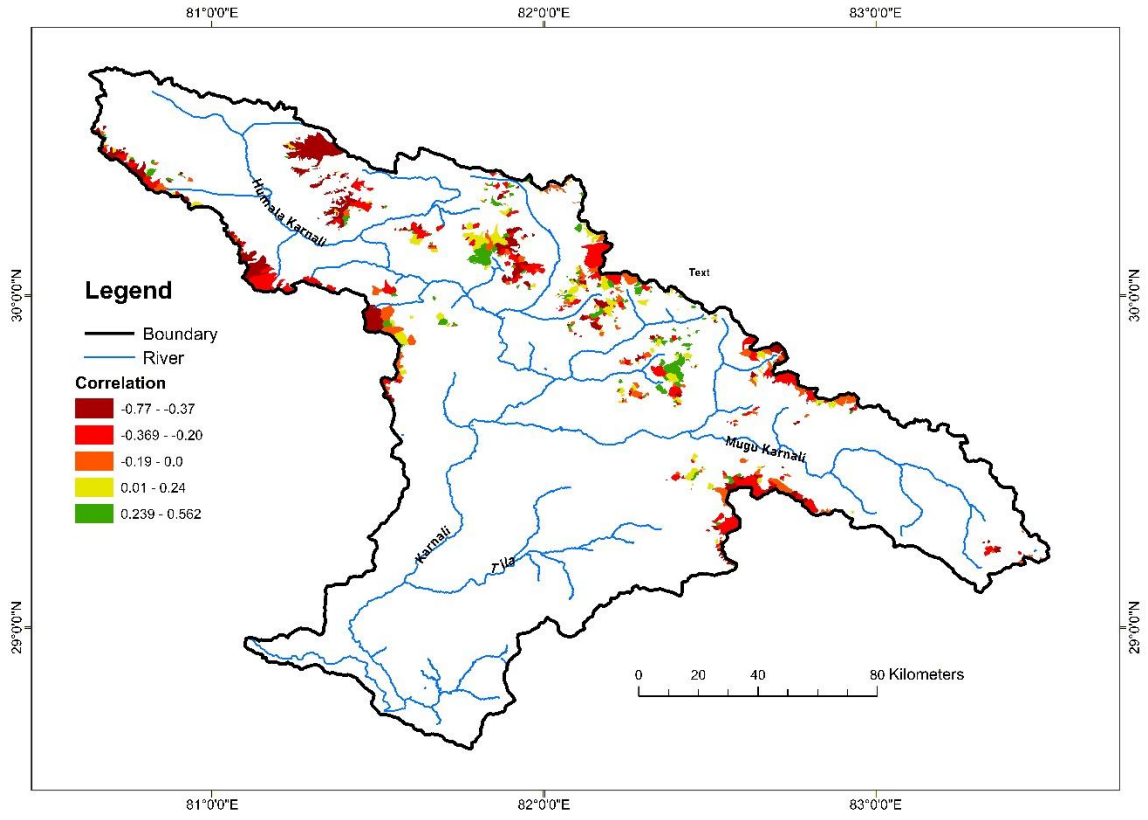


**Figure 12.** Snow cover trend on the Glacier Basins for January–March between 2000–2023 (Landsat 5, 7, and 8).

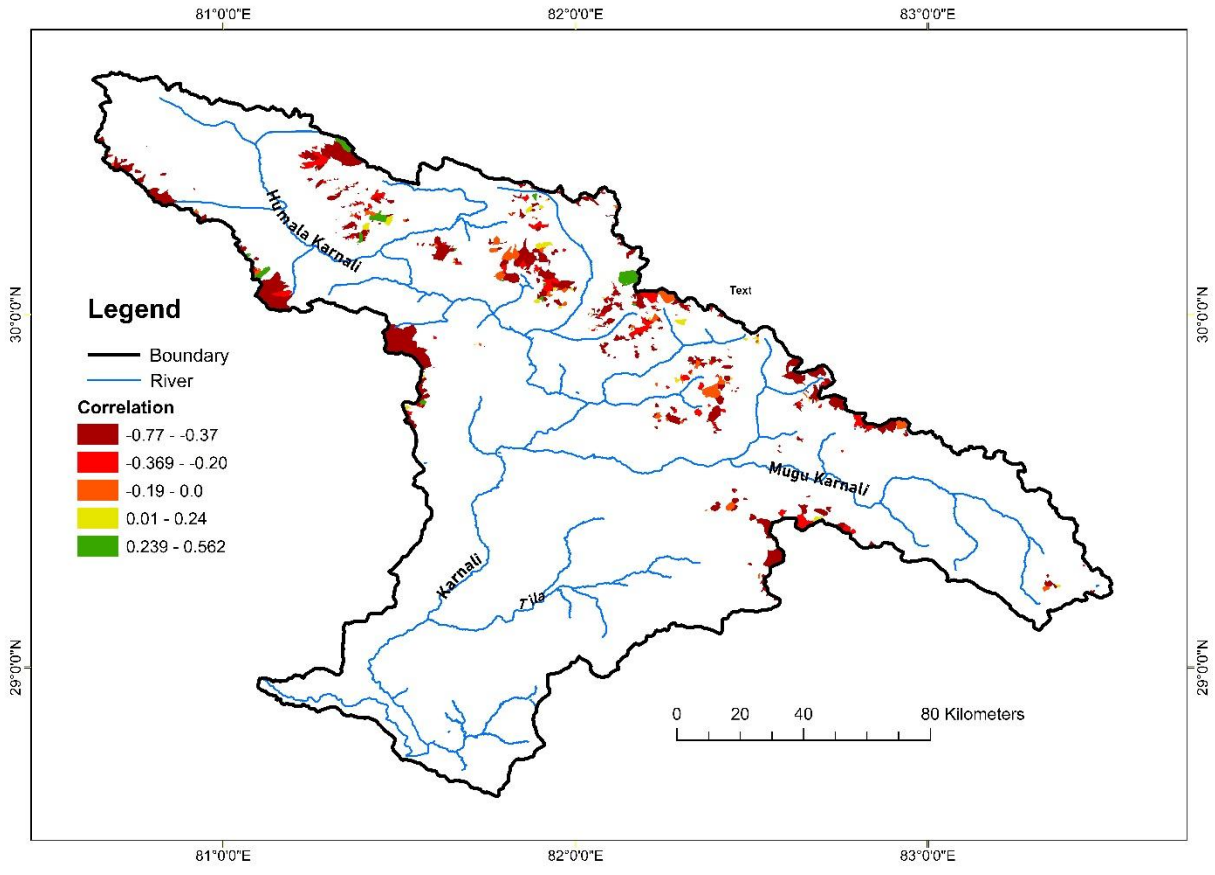


**Figure 13.** Snow cover trend on the glacier basins for October–December between 2000–2023 (Landsat 5, 7, and 8).

### 4.6. Snowline Shift across Elevations

Snow-covered areas were derived from the Landsat series 7, 8, and 9 by classifying snow using the Normalized Difference Snow Index (NDSI) algorithm to analyze changes in the snowline. This analysis was performed on the Google Earth Engine (GEE) platform. Snow pixels were identified with an NDSI threshold of > 0.4. The elevation-wise distribution of snow pixels was

then calculated. To determine the snowline's minimum elevation and its shift from 2002 to 2024, three statistical thresholds were applied: the 10th, 25th, and 50th percentiles of the snow cover distribution across various elevations.

The analysis of snowline altitude data from 2002 to 2024 reveals a significant upward trend across all percentiles (Figure 14). The 10th percentile shows the largest increase, with a Kendall's tau of 0.2662 and a Sen's slope of approximately 5.16 m/year, indicating that the lower snowline is rising quickly (Table 5). The 25th percentile presents a moderate yet statistically significant trend, with a Kendall's tau of 0.1938 and a Sen's slope of about 2.91 m/year. In contrast, the 50th percentile displays a gentler trend, with a Kendall's tau of 0.1483 and a Sen's slope of around 1.54 m/year, which remains statistically significant ($p<0.05$). Collectively, these findings suggest that the snowline is moving to higher elevations, reflecting broader climatic changes that affect lower elevations more intensively than the median snowline altitude.

**Table 5.** Statistical analysis of snow line altitude trends using Kendall's Tau and Sen's slope.

| Snow Line Percentile | Kendall's Tau | p-value | Sen's Slope (m/year) | Significance |
|---|---|---|---|---|
| 10th Percentile (SLA_10P) | 0.2662 | 0.00042 | 5.16 | Significant ($p < 0.001$) |
| 25th Percentile (SLA_25P) | 0.1938 | 0.01022 | 2.91 | Significant ($p < 0.05$) |
| 50th Percentile (SLA_50P) | 0.1483 | 0.04942 | 1.54 | Significant ($p < 0.05$) |

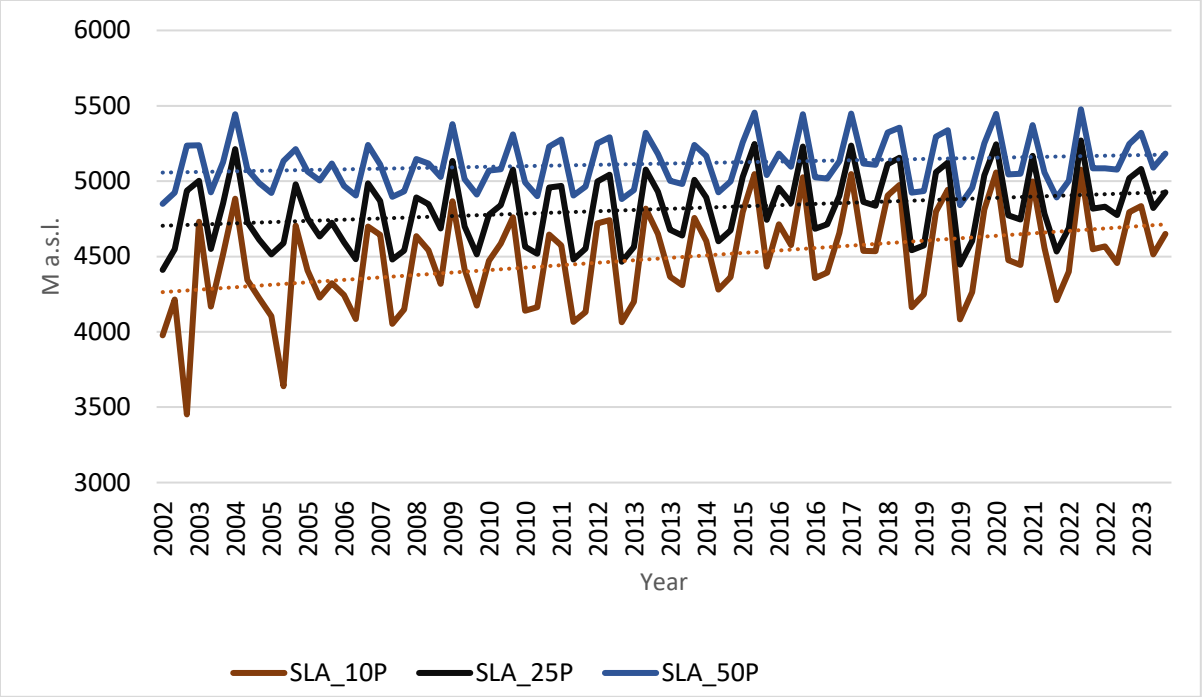


**Figure 14.** Snowline shift using snow line of elevation of 10, 25 and 50 percentile

## 5.0. Discussions

This study offers important insights into the interactions between snow and ice cover in the Upper Karnali Basin (UKB) and climatic and topographic factors. The results reveal notable trends and fluctuations in snow cover, glacial retreat, and the elevation of the snowline, aligning with the wider patterns of climate change seen in the Himalayan region. We will discuss the key findings below in relation to existing literature and their impact on water resources, ecosystems, and local communities.

The study on the Upper Karnali Basin from 2002 to 2024 reveals significant insights into the relationship between snow cover area (SCA), temperature, and precipitation. The annual average SCA is 872 km², with the highest snow cover occurring from January to March (1528 ± 333 km²)

and the lowest from July to September (169 ± 38.3 km²). The findings reveal a gradual decline in snow cover across the Upper Karnali Basin (UKB) from 2002 to 2024, with an average loss of ~3.99 km²/year.

There is a strong to moderate negative correlation between snow cover and temperature across all seasons ($r = -0.59$ to $-0.77$, $p < 0.05$), signifying that higher temperatures lead to reduced snow cover. In contrast, precipitation exhibits a positive correlation with snow cover in winter (January to March and October to December). The reduction in snow cover during winter months (January–March) indicates a potential shift in precipitation patterns, with more falling as rain instead of snow. The winter and pre-monsoon snowpack in the western Himalayas is heavily influenced by the Westerly wind system, which is a key source of snowfall in the UKB (Syed et al., 2006; Dimri & Dash, 2012). Consequently, the decline in winter snow cover may be due not only to temperature-induced changes in precipitation but also to a possible weakening or changing of the Westerlies, which needs to be further investigated. Such changes could lead to a decrease in overall moisture inflow (Yadav et al., 2009).

This shift is temperature-dependent and thus elevation-dependent, resulting in increased snowmelt, aligning with global warming trends (Wester et al., 2019). During the summer months (April to September), however, precipitation negatively correlates with snow cover, falling predominantly as rain, thus further enhancing snowmelt. Particularly, the period from July to September reveals a statistically significant decrease in snow cover (Sen's Slope = -2.87, $p<0.05$), primarily driven by warmer temperatures and higher rainfall during the summer monsoon, accelerating snowmelt.

Examining snow cover patterns in the UKB sub basins reveals notable seasonal and spatial differences. The Humla Karnali sub basin has the largest average snow cover during January–March, while downstream areas like Tila and Kawari exhibit less snow cover.

The interannual variability in snow cover highlights the sensitivity of snowpack to changing temperature and precipitation patterns. This variability significantly impacts water availability, as the observed reduction in snow cover could worsen water scarcity during the dry season, affecting millions who depend on snowmelt for irrigation, drinking water, and hydropower generation (Immerzeel et al., 2020; Pritchard, 2019). The strong negative correlation in Downstream Karnali ($r = -0.47$, $p < 0.05$) reinforces the declining trend in snow cover, which threatens water availability and ecosystem services in the region (Wester et al., 2019).

The outcomes emphasize the vulnerability of the UKB to climate change, with rising temperatures and shifting precipitation patterns leading to reduced snow cover. Adaptive water management strategies are essential to mitigate the impacts on water resources and local communities.

The findings on snow cover dynamics across elevation zones in the Upper Karnali Basin reveal significant elevation-dependent patterns, reflecting the influence of temperature fluctuations and global warming. At lower elevations (≤2000 m a.s.l.), snow cover exhibits a weak positive correlation (0.12–0.43), likely caused by occasional snowfall during short cold spells and a shift between rain and snow (Pendergrass, 2020). These zones experience high year-to-year variability (CoV ~41–43%), making trends less reliable, which should be interpreted with caution. Similar elevation-sensitive variability has also been reported in other Himalayan basins (Pepin et al., 2015).

The transition from weak negative correlations (snow cover by elevation and year) above 2300 m a.s.l. to the strongest negative correlation at 6100–6200 m a.s.l. (r = -0.56) corresponds with evidence of elevation-dependent warming (EDW), where higher altitudes experience accelerated warming, leading to reduced snow accumulation and increased melt rates. The sharp rise in mean snow cover above 5000 m a.s.l. coincides with permanent snow and glacier zones, but the decline in inter-annual variability (CoV) suggests a consistent reduction in snow cover, particularly at mid-to-high elevations (3000–5000 m a.s.l.).

The nonlinear relationship between elevation and inter-annual snow cover variability (CoV) proves particularly insightful. At 3000 m a.s.l. or below, the CoV reaches 41–43%, reflecting transitional zones where slight temperature fluctuations determine the precipitation phase (rain vs. snow). Above 3,000 m a.s.l., CoV drops to 25–30% as conditions remain persistently below freezing, but the dominant driver shifts to insolation and temperature-modulated melt rates. This aligns with Ren et al.'s (2023) findings on Tibetan Plateau glaciers, where albedo feedbacks dominate mass balance above 5000 m a.s.l.

The strong negative correlation between land surface temperature and snow cover (Tau = -0.43 to -0.79) highlights the impact of rising temperatures on snowpack. The most severe declines occur between 3000–5000 m a.s.l., where warming accelerates snowmelt and glacier retreat, threatening water availability for river flows, agriculture, and hydropower (Immerzeel et al., 2020; Bolch et al., 2012).

Between 2000 and 2023, glacier basins in the Upper Karnali Basin experienced significant ice and snow loss. The mean glacier area per basin declined from 119.04 to 100.47 hectares with an average loss of 18.6 hectares. While retreat was consistent across all aspects, north-facing basins (N, NW, NE) saw the largest total area decline. This trend, driven by rising temperatures and

reduced snowfall that create a negative mass balance (Pepin et al., 2022; Ren et al., 2024; Ye & Tian, 2022), threatens the persistence of glaciers and alters critical water resources.

Snow cover trends in glacier basins reveal a consistent decline across all seasons. From January to March, a majority (59%) of the 735 basins analyzed exhibit a statistically significant negative correlation ($p < 0.05$), with 16.3% of all basins showing a strong decline ($r < -0.44$). The trend is even more pronounced in the post-monsoon and ablation seasons (October–December). From July to September, 62% of basins (n=70) show a significant negative correlation, and in October–December, this figure rises to 91% (n=604). This widespread reduction in snow cover is linked to rising temperatures, which increase snowmelt rates and reduce albedo, further accelerating glacier retreat (Dowson et al., 2020). These trends underscore the vulnerability of the region's cryosphere to climate change, with serious implications for water security and regional hydrology.

The seasonal snowline in the Upper Karnali Basin is rising steadily, with rates of 5.6 m per year (10th percentile), 2.91 m per year (25th), and 1.54 m per year (50th). Although these are more conservative than many regional estimates, our findings align with the broader Himalayan trend of snowline elevation. Recent research reports faster increases, such as approximately 6.7–7.3 m per year in the Ganga–Brahmaputra basins (Dixit et al., 2024) and roughly 8–14 m per year in several Nepalese catchments (Sasaki et al., 2024), while the Langtang Basin shows a similar increase of about 2.2 m per year (Pradhananga et al., 2025). This suggests a consistent retreat of seasonal snow cover to higher elevations, which reduces the potential for snow accumulation to sustain glacier mass balance.

### 5.1. Feedback mechanisms and future projections

The correlation between temperature and snow cover (τ ranging from −0.43 to −0.79 across different elevations) confirms the presence of a reinforcing snow–albedo feedback in the Upper Karnali Basin (UKB). Increasing land surface temperatures reduces snow cover, lowering surface albedo and increasing shortwave radiation absorption. This process causes localized warming of about 0.8 to 1.2 °C, as estimated through Sen's slope analysis, further promoting melting and accelerating the feedback loop. Comparable snow–albedo feedback mechanisms have been observed across the central and eastern Himalayas (Kääb et al., 2015; Bolch et al., 2019; Bhattacharya et al., 2021; Salerno et al., 2021), underscoring the regional consistency of cryospheric amplification.

In addition to snow cover analysis, glacier change data (Ghimire, 2025) were integrated with long-term temperature and precipitation records to assess cryospheric variability. Relationships among temperature, snow cover, and glacier extent across elevation bands were quantified using Kendall's τ and Sen's slope, providing estimates of warming trends and snowline responsiveness. Future cryospheric conditions were simulated using a degree-day, elevation-band glacio-hydrological model forced with bias-corrected CMIP6 (NEX-GDDP) climate projections under the SSP1-2.6 and SSP2-4.5 scenarios, enabling projections of glacier and snow cover evolution through 2100 (Ghimire et al., 2025b)

Above 5,000 m a.s.l., Sen's slope analysis indicates a mean warming rate of +0.064 °C per year, comparable to the rates observed at mid-elevations (approximately +0.058 °C per year between 1,000 and 2,000 m). This elevation-dependent warming accelerates glacier thinning and shifts the snow–rain boundary upward, thereby reducing accumulation periods and causing earlier melt onset (Ghimire et. al., 2025). Similar warming trends, with mean annual temperature increases of

626 0.05–0.07 °C per year and glacier thinning rates of 0.3–1.0 m per year since 2000, have been
627 documented in the central Himalayas (Kääb et al., 2015; Bolch et al., 2019).

628 Under low-emission scenarios such as SSP1-2.6, high-altitude temperatures are projected to
629 increase by approximately 1 °C by 2100. Under the moderate SSP2-4.5 scenario, temperature
630 increases could reach 2 °C or more. Consequently, glacier areas are expected to decrease by 47–
631 69%. Snow-covered areas are projected to decline by 19–30%. (Ghimire et al., 2025b). This
632 would transform the basin's hydrology from nival (snowmelt-dominated) to pluvial (rain-
633 dominated), increasing flood risks during monsoons and drought susceptibility in dry seasons.

634 These projections align with other studies of Himalayan basins, which forecast reductions in
635 glacier area of 40–60% by mid-century (Bhattacharya et al., 2021; Salerno et al., 2021; Hock et
636 al., 2019). Comparable amplification mechanisms are also evident in the Andes and Alps, where
637 rapid glacier retreat and albedo-induced warming mirror trends observed in the Himalayas
638 (Rabatel et al., 2013; Vuille et al., 2018; Dussaillant et al., 2019; Beniston & Stoffel, 2014; Zemp
639 et al., 2019; Zekollari et al., 2019).

640 **6.0. Conclusions**

641 The study of snow and glacier cover dynamics in the Upper Karnali Basin from 2002 to 2024
642 reveals a persistent decline in snow cover, glacier area, and snowline elevation, driven by rising
643 temperatures and altered precipitation patterns.

644 The annual snow-covered area (SCA) has decreased by approximately 3.99 km² per year, with
645 the most significant reductions observed during the July-September monsoon period. The decline
646 in snow cover is statistically correlated with increasing temperatures, demonstrating the impact

of climate change on seasonal snow accumulation and melt cycles. The winter snow cover variability suggests changes in snowfall patterns rather than a uniform decrease.

Notable seasonal and spatial differences in snow cover patterns are observed in the Sub basins of UKB for two seasons, January–March and October–December. The upstream sub basins experience less inconsistent snowfall than the downstream basins. During October–December, snowfall is inconsistent in all basins, but more inconsistent in particularly China Karnali, Tila and Downstream Karnali.

Elevation-dependent trend analysis confirms that snow cover at lower elevations (<2000 m a.s.l.) exhibits high interannual variability, while higher elevations (>3000 m a.s.l.) show a significant long-term decline. The strongest reductions occur between 3000–5000 m a.s.l., where warming accelerates snowmelt and glacier retreat. The observed negative correlation between snow cover and rising temperatures confirms the climate-driven reduction in snowpack, exacerbating the risk of water shortages.

The study of glacier basins shows widespread retreat, with the mean glacier area declining from 119.05 hectares in 2000 to 100.47 hectares in 2023. Glacier retreat is most pronounced in north-facing basins (N, NW, NE), where melting exceeds accumulation. The continuous decline in snow cover across glacier basins indicates an ongoing negative mass balance, threatening long-term glacier persistence.

Additionally, the snow line is gradually shifting upward, with the 10th, 25th, and 50th percentiles rising by approximately 5.16, 2.91, and 1.54 meters per year, respectively, indicating a consistent loss of seasonal snow accumulation.

Given the current warming trends (~0.0643°C/year above 5000 m a.s.l.), the UKB could experience a decline of glacier area by 47–69 % and snow-covered area by 19–30 %. This would transform the hydrology from snowmelt-dominated (nival) to rainfall-dominated (pluvial), increasing the frequency of extreme weather events and altering regional water security dynamics. The findings emphasize the need for proactive water resource management, improved climate resilience strategies, and continuous monitoring of cryospheric changes to mitigate future risks. Policymakers must prioritize adaptation measures, such as improved water storage infrastructure and sustainable land-use practices, to ensure long-term water security in the Upper Karnali Basin and beyond.

## Author contributions

MG conceptualized the research, designed the methodology, conducted fieldwork, analyzed the data, and drafted the manuscript. DS. and RC assisted in proposal writing, research design, fieldwork, and data analysis. AT, TPPS, KPS, SBG, and SD contributed to procuring remote sensing and climate data. PB and SK were responsible for procuring and updating MODIS data. WY reviewed the manuscript and provided feedback to enhance its quality. NT and JK assisted in GIS analysis. All authors contributed to revising the manuscript and provided input before submission.

## Competing Interests

The authors declare that they have no conflict of interest.

## Data availability

MODIS, Landsat, Sentinel, ERA5 renalysis climate datasets, and NEX-GDDP data are publicly available.

## Acknowledgments

We express our gratitude to the Director of Tribhuvan University's Research Coordination and Development Council (RCDC) for supporting the project titled "State and Dynamics of the Cryosphere of the Upper Karnali Basin, Associated Hazards and Implications for Water Resources and Livelihood" (Project Code TU-NPAR-077/78-ERG-15). This paper is a product of that project. We appreciate the Evaluation and Monitoring Committee of RCDC for their insightful feedback and suggestions, which greatly enhanced the manuscript. We also thank the University Grants Commission for providing research funding. Authors would also like to sincerely acknowledge the Sichuan Science and Technology Program (2024YFHZ0248) for partial support. We also acknowledge the contributions of Google Earth Engine, ERA5, ESRI, and other open-access resources for providing satellite imagery and data.

## Financial support

This research was funded by the University Grants Commission (UGC), Kathmandu, through Tribhuvan University's Research Coordination and Development Council (RCDC) under the National Policy Area Research program. The Sichuan Science and Technology Program (2024YFHZ0248) also provided partial funding for this research.

## References

Anup, K.: Climate change and its impact on tourism in Nepal, J. Tour. Hosp. Educ., 7, 25–43, https://doi.org/10.3126/jthe.v7i0.17693, 2017.

Bajracharya, S. R., Bajracharya, O. R., Baidya, S., Maharjan, S. B., and Shrestha, F.: Climate change impact on glaciers in the Langtang and Imja sub-basins of Nepal from late 70s to 2010, in: AGU Fall Meeting Abstracts, San Francisco, CA, 15–19 December, C31B-0278, 2014.

712

713 Beniston, M. and Stoffel, M.: Assessing the impacts of climatic change on mountain water
714 resources, Sci. Total Environ., 493, 1129–1137, https://doi.org/10.1016/j.scitotenv.2013.11.122,
715 2014.

716 Bhattacharya, A., Bolch, T., Mukherjee, K., King, O., Menounos, B., Kapitsa, V., Neckel, N.,
717 Yao, T., and Li, X.: High Mountain Asian glacier response to climate revealed by multi-temporal
718 satellite observations since the 1960s, Nat. Commun., 12, 4133, https://doi.org/10.1038/s41467-
719 021-24180-y, 2021.

720 Bolch, T., Buchroithner, M. F., Kunert, A., and Kamp, U.: Automated delineation of debris-
721 covered glaciers based on ASTER data, in: GeoInformation in Europe, edited by: Gomarasca, M.
722 A., Millpress, Rotterdam, 403–410, 2007.

723 Bolch, T., Kulkarni, A., Kääb, A., Huggel, C., Paul, F., Cogley, J. G., Frey, H., Kargel, J. S.,
724 Fujita, K., Scheel, M., Bajracharya, S., and Stoffel, M.: The state and fate of Himalayan glaciers,
725 Science, 336, 310–314, https://doi.org/10.1126/science.1215828, 2012.

726 Bookhagen, B. and Burbank, D. W.: Toward a complete Himalayan hydrological budget:
727 Spatiotemporal distribution of snowmelt and rainfall and their impact on river discharge, J.
728 Geophys. Res.-Earth Surf., 115, F03019, https://doi.org/10.1029/2009JF001426, 2010.

729 CBS: National Population and Housing Census 2021 – Province 6 (Karnali) results (online
730 tables), Central Bureau of Statistics, Nepal, 2021.

731 Desinayak, S., Shrestha, M. S., Gurung, D. R., and Murthy, M. S. R.: Recent changes in snow
732 cover extent over the Hindu Kush Himalaya, Int. J. Climatol., 42, 6789–6803,
733 https://doi.org/10.1002/joc.7038, 2022.

734 Dimri, A. P. and Dash, S. K.: Wintertime climatic trends in the western Himalayas, Clim.
735 Change, 111, 775–800, https://doi.org/10.1007/s10584-011-0201-y, 2012.

736 Dixit, A., Goswami, A., Jain, S., and Das, P.: Assessing snow cover patterns in the Indus–
737 Ganga–Brahmaputra River Basins of the Hindu Kush Himalayas using snow persistence and
738 snow line as metrics, Environ. Chall., 14, 100834, https://doi.org/10.1016/j.envc.2023.100834,
739 2024.

740 Dhital, M. R.: Geology of the Nepal Himalaya: Regional Perspective, Springer International
741 Publishing, Cham, Switzerland, 583 pp., https://doi.org/10.1007/978-3-319-02496-7, 2015.

742 Dowson, A. J., Sirguey, P., and Cullen, N. J.: Variability in glacier albedo and links to annual
743 mass balance for the Gardens of Eden and Allah, Southern Alps, New Zealand, The Cryosphere,
744 14, 3425–3448, https://doi.org/10.5194/tc-14-3425-2020, 2020.

745 Duan, S.-B., Li, Z.-L., Li, H., Göttsche, F.-M., Wu, H., Zhao, W., Leng, P., Zhang, X., and Coll,
746 C.: Validation of Collection 6 MODIS land surface temperature product using in situ
747 measurements, Remote Sens. Environ., 225, 16–29, https://doi.org/10.1016/j.rse.2019.02.020,
748 2019.

749 Dussaillant, I., Berthier, E., Brun, F., Masiokas, M., Hugonnet, R., Favier, V., Rabatel, A., Pitte,
750 P., and Ruiz, L.: Two decades of glacier mass loss along the Andes, Nat. Geosci., 12, 802–808,
751 https://doi.org/10.1038/s41561-019-0432-5, 2019.

752 Elsasser, H. and Bürki, R.: Climate change as a threat to tourism in the Alps, Clim. Res., 20,
753 253–257, https://doi.org/10.3354/cr020253, 2002.

754 Forster, P., Storelvmo, T., Armour, K., Collins, W., Dufresne, J.-L., Frame, D., Lunt, D. J.,
755 Mauritsen, T., Palmer, M. D., Watanabe, M., and Wild, M.: The Earth's Energy Budget, Climate
756 Feedbacks, and Climate Sensitivity, in: Climate Change 2021: The Physical Science Basis.
757 Contribution of Working Group I to the Sixth Assessment Report of the Intergovernmental Panel
758 on Climate Change, edited by: Masson-Delmotte, V., Zhai, P., Pirani, A., Connors, S. L., Péan,
759 C., Berger, S., Caud, N., Chen, Y., Goldfarb, L., Gomis, M. I., Huang, M., Leitzell, K., Lonnoy,
760 E., Matthews, J. B. R., Maycock, T. K., Waterfield, T., Yelekçi, Ö., Yu, R., and Zhou, B.,
761 Cambridge University Press, Cambridge, UK and New York, NY, USA, 923–1054,
762 https://doi.org/10.1017/9781009157896.009, 2021.

763 Gafurov, A. and Bárdossy, A.: Cloud removal methodology from MODIS snow cover product,
764 Hydrol. Earth Syst. Sci., 13, 1361–1373, https://doi.org/10.5194/hess-13-1361-2009, 2009.

765 Gilbert, R. O.: Statistical Methods for Environmental Pollution Monitoring, Van Nostrand
766 Reinhold, New York, 272 pp., 1987.

767 Gorelick, N., Hancher, M., Dixon, M., Ilyushchenko, S., Thau, D., and Moore, R.: Google Earth
768 Engine: Planetary-scale geospatial analysis for everyone, Remote Sens. Environ., 202, 18–27,
769 https://doi.org/10.1016/j.rse.2017.06.031, 2017.

770 Gurung, D. R., Maharjan, S. B., Shrestha, A. B., Shrestha, M. S., Bajracharya, S. R., and Murthy,
771 M. S. R.: Climate and topographic controls on snow cover dynamics in the Hindu Kush
772 Himalaya, Int. J. Climatol., 37, 3873–3882, https://doi.org/10.1002/joc.5063, 2017.

773 Hall, D. K., Riggs, G. A., Salomonson, V. V., DiGirolamo, N. E., and Bayr, K. J.: MODIS snow-
774 cover products, Remote Sens. Environ., 83, 181–194, https://doi.org/10.1016/S0034-
775 4257(02)00095-0, 2002.

776 Heid, T. and Kääb, A.: Evaluation of existing image matching methods for deriving glacier
777 surface displacements from repeat optical satellite images, Remote Sens. Environ., 118, 339–
778 355, https://doi.org/10.1016/j.rse.2011.11.025, 2012.

779 Hersbach, H., Bell, B., Berrisford, P., Hirahara, S., Horányi, A., Muñoz-Sabater, J., Nicolas, J.,
780 Peubey, C., Radu, R., Schepers, D., Simmons, A., Soci, C., Abdalla, S., Abellan, X., Balsamo,
781 G., Bechtold, P., Biavati, G., Bidlot, J., Bonavita, M., De Chiara, G., Dahlgren, P., Dee, D.,
782 Diamantakis, M., Dragani, R., Flemming, J., Forbes, R., Fuentes, M., Geer, A., Haimberger, L.,
783 Healy, S., Hogan, R. J., Hólm, E., Janisková, M., Keeley, S., Laloyaux, P., Lopez, P., Lupu, C.,
784 Radnoti, G., de Rosnay, P., Rozum, I., Vamborg, F., Villaume, S., and Thépaut, J.-N.: The ERA5
785 global reanalysis, Q. J. R. Meteorol. Soc., 146, 1999–2049, https://doi.org/10.1002/qj.3803,
786 2020.

787 Hock, R., Rasul, G., Adler, C., Cáceres, B., Gruber, S., Hirabayashi, Y., Jackson, M., Kääb, A.,
788 Kang, S., Kutuzov, S., Milner, A., Molau, U., Morin, S., Orlove, B., and Steltzer, H.: High
789 Mountain Areas, in: IPCC Special Report on the Ocean and Cryosphere in a Changing Climate,
790 edited by: Pörtner, H.-O., Roberts, D. C., Masson-Delmotte, V., Zhai, P., Tignor, M.,
791 Poloczanska, E., Mintenbeck, K., Alegría, A., Nicolai, M., Okem, A., Petzold, J., Rama, B., and
792 Weyer, N. M., Cambridge University Press, Cambridge, UK and New York, NY, USA, 131–
793 202, https://doi.org/10.1017/9781009157964.004, 2019.

794 Hunt, K. M. R., Turner, A. G., and Schiemann, R. K. H.: Western disturbances: a review,
795 Weather Clim. Dynam., 6, 43–65, https://doi.org/10.5194/wcd-6-43-2025, 2025.

796 Ghimire, M., Pangali Sharma, T. P., Chauhan, R., Gurung, S. B., Devkota, S., Sharma, K. P.,
797 Shrestha, D., Wei, Z., and Timalsina, N.: Status and changes in glaciers in the Upper Karnali
798 Basin, West Nepal: Assessing topographic influences on area, fragmentation, and volume, J.
799 Earth Syst. Sci., https://doi.org/10.1007/s12040-025-02664-5, 2025a.

800 Ghimire, M., Shrestha, D., Zhao, W., Chauhan, R., Gurung, S. B., Pangali Sharma, T. P.,
801 Sharma, K. P., Tamang, S., Timaisina, N., Devkota, S., Thapa, A., Koirala, S., Bhandari, P.,
802 Subedi, B., Lohani, U., Kutu, J., Rana, D., and Yanhong, W.: State and Dynamics of Cryosphere
803 of Upper Karnali Basin, Associated Hazards and Implications to Water Resources and
804 Livelihood, Project Code TU-NPAR-077/78-ERG-15, Tribhuvan University, Research
805 Coordination and Development Council (RCDC), Kathmandu, Nepal, 2025b.

806 Immerzeel, W. W., Lutz, A. F., Andrade, M., Bahl, A., Biemans, H., Bolch, T., Hyde, S.,
807 Brumby, S., Davies, B. J., Elmore, A. C., Emmer, A., Feng, M., Fernández, A., Haritashya, U.,
808 Kargel, J. S., Koppes, M., Kraaijenbrink, P. D. A., Kulkarni, A. V., Mayewski, P. A., Nepaul, S.,
809 Pacheco, P., Pak-sok, J., Poulton, C., Pradhan, S., Rangecroft, S., Smeets, S., Suzuki, T., van der
810 Schriek, T., Viviroli, D., Wada, Y., Xiao, C., Yao, T., and Baillie, J. E. M.: Importance and
811 vulnerability of the world's water towers, Nature, 577, 364–369, https://doi.org/10.1038/s41586-
812 019-1822-y, 2020.

813 Kääb, A., Berthier, E., Nuth, C., Gardelle, J., and Arnaud, Y.: Contrasting patterns of early
814 twenty-first-century glacier mass change in the Himalayas, Nature, 488, 495–498,
815 https://doi.org/10.1038/nature11324, 2012.

816 Kääb, A., Reynolds, J. M., and Haeberli, W.: Glacier and permafrost hazards in high mountains,
817 in: Global Change and Mountain Regions, edited by: Huber, U. M., Bugmann, H. K. M., and
818 Reasoner, M. A., Springer, Dordrecht, 225–234, https://doi.org/10.1007/1-4020-3508-X_23,
819 2005.

820 Khadka, N., Li, B., Wu, Q., Shrestha, F., Paudel, L., and Wang, W.: Glacial lake outburst floods
821 threaten China–Nepal transportation corridors, Sci. Total Environ., 927, 172456,
822 https://doi.org/10.1016/j.scitotenv.2024.172456, 2024.

823 Khatiwada, K. R., Panthi, J., Shrestha, M. L., and Nepal, S.: Hydro-climatic variability in the
824 Karnali River basin of Nepal Himalaya, Climate, 4, 17, https://doi.org/10.3390/cli4020017,
825 2016.

826 Krishnan, R., Shrestha, A. B., Ren, G., Rajbhandari, R., Saeed, S., Sanjay, J., Syed, M. A.,
827 Vellore, R., Xu, Y., You, Q., and Ren, Y.: Unravelling climate change in the Hindu Kush
828 Himalaya: rapid warming in the mountains and increasing extremes, in: The Hindu Kush
829 Himalaya Assessment: Mountains, Climate Change, Sustainability and People, edited by:
830 Wester, P., Mishra, A., Mukherji, A., and Shrestha, A. B., Springer International Publishing,
831 Cham, 57–97, https://doi.org/10.1007/978-3-319-92288-1_3, 2019.

832 Kulkarni, A. V., Rathore, B. P., and Singh, S. K.: Distribution of seasonal snow cover in central
833 and western Himalaya, Ann. Glaciol., 51, 125–130,
834 https://doi.org/10.3189/172756410791386445, 2010.

835 Kulkarni, A. V., Shirsat, T. S., Kulkarni, A., Negi, H. S., Bahuguna, I. M., and Thamban, M.:
836 State of Himalayan cryosphere and implications for water security, Water Security, 14, 100101,
837 https://doi.org/10.1016/j.wasec.2021.100101, 2021.

LRMP: Land Resource Mapping Project (national soils/land-use inventory), Government of Nepal, Kathmandu, Nepal, 1986.

Maskey, S., Thapa, B., and Rijal, K.: Snow cover variability and snowmelt in the Himalayan region: A study using MODIS snow products, J. Hydrol. Meteorol., 8, 1–10, https://doi.org/10.3126/jhm.v8i1.5920, 2011b.

Maskey, S., Uhlenbrook, S., and Ojha, S.: An analysis of snow cover changes in the Himalayan region using MODIS snow products and in-situ temperature data, Clim. Change, 108, 391–400, https://doi.org/10.1007/s10584-011-0033-6, 2011a.

Mimura, N.: Sea-level rise caused by climate change and its implications for society, Proc. Jpn. Acad. Ser. B, 89, 281–301, https://doi.org/10.2183/pjab.89.281, 2013.

Muhammad, S. and Thapa, A.: An improved Terra–Aqua MODIS snow cover and Randolph Glacier Inventory 6.0 combined product (MOYDGL06*) for high-mountain Asia between 2002 and 2018, Earth Syst. Sci. Data, 12, 345–356, https://doi.org/10.5194/essd-12-345-2020, 2020.

Naegeli, K., Huss, M., and Hoelzle, M.: Change detection of bare-ice albedo in the Swiss Alps, The Cryosphere, 13, 397–412, https://doi.org/10.5194/tc-13-397-2019, 2019.

Nyaupane, G. P. and Chhetri, N.: Vulnerability to climate change of nature-based tourism in the Nepalese Himalayas, Tour. Geogr., 11, 95–119, https://doi.org/10.1080/14616680802643359, 2009.

Pradhananga, D., Adhikary, S., Dhakal, B. N., Dhakal, A., Ghimire, A., Dhital, S., and Manandhar, S.: Cryosphere change in the warming Himalaya: Snow cover and snowline trends in Nepal's Langtang Basin (1988–2024), J. Tourism Himalayan Adv., 7, 14–26, 2025.

Parajka, J. and Blöschl, G.: Spatio-temporal combination of MODIS images – Potential for snow cover mapping, Water Resour. Res., 44, W03406, https://doi.org/10.1029/2007WR006208, 2008.

Parris, A. S., Bromirski, P., Burkett, V., Cayan, D. R., Culver, M. E., Hall, J., Horton, R. M., Knuuti, K., Moss, R. H., Obeysekera, J., Sallenger, A. H., and Weiss, J. L.: Global Sea Level Rise Scenarios for the United States National Climate Assessment, NOAA Tech. Memo. OAR CPO-1, 37 pp., 2012.

Pendergrass, A. G.: Changing degree of convective organization as a mechanism for dynamic changes in extreme precipitation, Curr. Clim. Change Rep., 6, 47–54, https://doi.org/10.1007/s40641-020-00156-z, 2020.

Pepin, N. C., Arnone, E., Gobiet, A., Haslinger, K., Kotlarski, S., Notarnicola, C., Palazzi, E., Seibert, P., Serafin, S., Stocchi, P., and Zebisch, M.: Climate changes and their elevational patterns in the mountains of the world, Rev. Geophys., 60, e2020RG000730, https://doi.org/10.1029/2020RG000730, 2022.

Pepin, N., Bradley, R. S., Diaz, H. F., Baraer, M., Caceres, E. B., Forsythe, N., Fowler, H., Greenwood, G., Hashmi, M. Z., Liu, X. D., Miller, J. R., Ning, L., Ohmura, A., Palazzi, E., Rangwala, I., Schöner, W., Severskiy, I., Shahgedanova, M., Wang, M. B., Williamson, S. N., and Yang, D. Q.: Elevation-dependent warming in mountain regions of the world, Nat. Clim. Change, 5, 424–430, https://doi.org/10.1038/nclimate2563, 2015.

Pfeffer, W. T., Arendt, A. A., Bliss, A., Bolch, T., Cogley, J. G., Gardner, A. S., Hagen, J.-O., Hock, R., Kaser, G., Kienholz, C., Miles, E. S., Moholdt, G., Mölg, N., Paul, F., Radic, V., Rastner, P., Raup, B. H., Rich, J., Sharp, M. J., and the Randolph Consortium: The Randolph

Glacier Inventory: a globally complete inventory of glaciers, J. Glaciol., 60, 537–552, https://doi.org/10.3189/2014JoG13J176, 2014.

Pritchard, H. D.: Asia's shrinking glaciers protect large populations from drought stress, Nature, 569, 649–654, https://doi.org/10.1038/s41586-019-1240-1, 2019.

Ren, P., Pan, X., Liu, T., Huang, Y., Chen, X., Wang, X., Zhang, Y., and Ling, X.: Glacier changes from 1990 to 2022 in the Aksu River Basin, western Tien Shan, Remote Sens., 16, 1751, https://doi.org/10.3390/rs16101751, 2024.

Ren, S., Jia, L., Menenti, M., and Zhang, J.: Changes in glacier albedo and the driving factors in the Western Nyainqentanglha Mountains from 2001 to 2020, J. Glaciol., 69, 1500–1514, https://doi.org/10.1017/jog.2023.33, 2023.

Rittger, K., Painter, T. H., and Dozier, J.: Assessment of methods for mapping snow cover from MODIS, Adv. Water Resour., 51, 367–380, https://doi.org/10.1016/j.advwatres.2012.03.002, 2013.

Salerno, F., Uccelli, A., Cristofanelli, P., Stocchi, P., Diolaiuti, G., Ma, Y., and Putero, D.: Local cooling and drying induced by Himalayan glaciers, Nat. Geosci., 16, 1120–1127, https://doi.org/10.1038/s41561-023-01331-y, 2023.

Sasaki, O., Miles, E. S., Pellicciotti, F., Sakai, A., and Fujita, K.: Contrasting patterns of change in snowline altitude across five Himalayan catchments, *EGUsphere* [preprint], https://doi.org/10.5194/egusphere-2024-2026, 2024.

Sen, P. K.: Estimates of the regression coefficient based on Kendall's tau, J. Am. Stat. Assoc., 63, 1379–1389, https://doi.org/10.1080/01621459.1968.10480934, 1968.

Shen, L., Zhang, Y., Ullah, S., Pepin, N., and Ma, Q.: Changes in snow depth under elevation-dependent warming over the Tibetan Plateau, Atmos. Sci. Lett., 22, e1041, https://doi.org/10.1002/asl.1041, 2021.

Shrestha, M., Wang, L., Koike, T., Xue, Y., and Hirabayashi, Y.: Modeling the spatial distribution of snow cover in the Dudhkoshi region of the Nepal Himalayas, J. Hydrometeorol., 13, 204–222, https://doi.org/10.1175/JHM-D-10-05005.1, 2012.

Syed, F. S., Giorgi, F., Pal, J. S., and King, M. P.: Effect of remote forcings on the winter precipitation of central southwest Asia part 1: observations, Theor. Appl. Climatol., 86, 147–160, https://doi.org/10.1007/s00704-005-0217-1, 2006.

Vuille, M., Carey, M., Huggel, C., Buytaert, W., Rabatel, A., Jacobsen, D., Soruco, A., Villacis, M., Yarleque, C., Elison Timm, O., Condom, T., Salzmann, N., and Sicart, J. E.: Rapid decline of snow and ice in the tropical Andes – Impacts, uncertainties and challenges ahead, Earth-Sci. Rev., 176, 195–213, https://doi.org/10.1016/j.earscirev.2017.09.019, 2018.

Wan, Z., Hook, S., and Hulley, G.: MODIS/Aqua Land Surface Temperature/Emissivity Daily L3 Global 1km SIN Grid, Version 6, NASA EOSDIS Land Processes DAAC, https://doi.org/10.5067/MODIS/MYD11A1.006, 2015.

Wester, P., Mishra, A., Mukherji, A., and Shrestha, A. B. (Eds.): The Hindu Kush Himalaya Assessment: Mountains, Climate Change, Sustainability and People, Springer Nature, Cham, Switzerland, 627 pp., https://doi.org/10.1007/978-3-319-92288-1, 2019.

Xu, J., Grumbine, R. E., Shrestha, A., Eriksson, M., Yang, X., Wang, Y., and Wilkes, A.: The melting Himalayas: cascading effects of climate change on water, biodiversity, and livelihoods, Conserv. Biol., 23, 520–530, https://doi.org/10.1111/j.1523-1739.2009.01237.x, 2009.

Yadav, R. K., Rupa Kumar, K., and Rajeevan, M.: Increasing influence of ENSO and decreasing influence of AO/NAO in the recent decades over northwest India winter precipitation, *J. Geophys. Res.-Atmos.*, 114, D12112, https://doi.org/10.1029/2008JD011318, 2009.

Ye, Y. and Tian, Y.: Interpreting changes in albedo and mass balance at White Glacier, Canadian Arctic Archipelago, Int. Arch. Photogramm. Remote Sens. Spat. Inf. Sci., XLIII-B3-2022, 793–798, https://doi.org/10.5194/isprs-archives-XLIII-B3-2022-793-2022, 2022.

Yu, W., Ma, M., Wang, X., Geng, L., Tan, J., and Shi, J.: Validation of MODIS land surface temperature products using ground-based longwave radiation observations in the Heihe River Basin, Proc. SPIE, 8174, 81741G, https://doi.org/10.1117/12.898243, 2011.

Yue, S. and Wang, C. Y.: The Mann–Kendall test modified by effective sample size to detect trend in serially correlated hydrological series, Water Resour. Manag., 18, 201–218, https://doi.org/10.1023/B:WARM.0000043140.61082.60, 2004.

Zemp, M., Huss, M., Thibert, E., Eckert, N., McNabb, R., Huber, J., Barandun, M., Machguth, H., Nussbaumer, S. U., Gärtner-Roer, I., Thomson, L., Paul, F., Maussion, F., Kutuzov, S., and Cogley, J. G.: Global glacier mass changes and their contributions to sea-level rise from 1961 to 2016, Nature, 568, 382–386, https://doi.org/10.1038/s41586-019-1071-0, 2019.

Zemp, M., Roer, I., Kääb, A., Hoelzle, M., Paul, F., and Haeberli, W. (Eds.): Global glacier changes: facts and figures, United Nations Environment Programme and World Glacier Monitoring Service, Nairobi, Kenya and Zurich, Switzerland, 88 pp., 2008.

Zhao, B., Mao, K., Cai, Y., Shi, J., Li, Z., Qin, Z., Meng, X., Shen, X., and Guo, Z.: A combined Terra and Aqua MODIS land surface temperature and meteorological station data product for

China from 2003 to 2017, Earth Syst. Sci. Data, 12, 2555–2577, https://doi.org/10.5194/essd-12-2555-2020, 2020.

Zhao, W., He, J., Wu, Y., Xiong, D., Wen, F., and Li, A.: An analysis of land surface temperature trends in the central Himalayan region based on MODIS products. Remote Sensing, 11(8), 900.https://doi.org/10.3390/rs11080900, 2019.